ANALYSIS OF THE EFFECT OF ELEMENT RADIATION PATTERN IN THE PERFORMANCE OF MIMO ARRAYS USED IN IMAGING APPLICATIONS

A THESIS SUBMITTED TO
THE GRADUATE SCHOOL OF NATURAL AND APPLIED SCIENCES
OF
MIDDLE EAST TECHNICAL UNIVERSITY

BY

FIRAT ALTUNTAŞ

IN PARTIAL FULFILLMENT OF THE REQUIREMENTS
FOR
THE DEGREE OF MASTER OF SCIENCE
IN
ELECTRICAL AND ELECTRONIC ENGINEERING

SEPTEMPER 2020

Approval of the thesis:

ANALYSIS OF THE EFFECT OF ELEMENT RADIATION PATTERN IN THE PERFORMANCE OF MIMO ARRAYS USED IN IMAGING APPLICATIONS

submitted by **FIRAT ALTUNTAŞ** in partial fulfillment of the requirements for the degree of **Master of Science** i**n Electrical and Electronic Engineering, Middle East Technical University** by,

Prof. Dr. Halil Kalıpçılar
Dean, Graduate School of **Natural and Applied Sciences** _____

Prof. Dr. İlkay Ulusoy
Head of the Department, **Electrical and Electronic Engineering** _____

Assoc. Prof. Dr. Lale Alatan
Supervisor, **Electrical and Electronic Engineering, METU** _____

Examining Committee Members:

Prof. Dr. Gülbin Dural
Electrical and Electronics Eng. Dept., METU _____

Assoc. Prof. Dr. Lale Alatan
Electrical and Electronics Eng. Dept., METU _____

Prof. Dr. Sencer Koç
Electrical and Electronics Eng. Dept., METU _____

Prof. Dr. Özlem Aydın Çivi
Electrical and Electronics Eng. Dept., METU _____

Prof. Dr. Vakur B. Ertürk
Electrical and Electronics Eng. Dept., Bilkent University _____

Date:21.09.2020

I hereby declare that all information in this document has been obtained and presented in accordance with academic rules and ethical conduct. I also declare that, as required by these rules and conduct, I have fully cited and referenced all material and results that are not original to this work.

Name, Last name : Fırat Altuntaş

Signature :

ABSTRACT

ANALYSIS OF THE EFFECT OF ELEMENT RADIATION PATTERN IN THE PERFORMANCE OF MIMO ARRAYS USED IN IMAGING APPLICATIONS

Altuntaş, Fırat
Master of Science, Electrical and Electronic Engineering
Supervisor : Assoc. Prof. Dr. Lale Alatan

September 2020, 69 pages

Along with the developments in technology, complexity of the systems tends to increase. Consequently rigorous models that take into account of all the effects in such complex systems become very time consuming. In this study, an ultra-wide band (UWB) multi-input multi-output (MIMO) imaging system is considered and a simple model that is generally used in the analysis of such systems is improved with an effort to obtain results closer to those achieved by rigorous models. Simple or rigorous models simulates the data that is received by a receiver antenna when a specified target is illimunated by a transmitter antenna. After obtaining this data for all transmitter receiver pairs, the point spread function (PSF) of the system can be obtained with the utilization of back projection method. In order to verify the proper operation of the implemented simple model, UWB signal characteristics and antenna configuration in the array aperture are analyzed and the results are compared with those found in the literature. After verifying the proper operation of the implemented simple model, antenna radiation pattern is embedded into the calculations and an improved model is obtained. By comparing point spread functions obtained by using the data generated by improved and rigorous models, effect of element radiation pattern on multi-input multi-output (MIMO) imaging

system is examined. In this thesis, full-wave electromagnetic simulation software CST Studio is used to generate the data of the rigorous model.

Keywords: MIMO, UWB, Back Projection, Point Spread Function

ÖZ

GÖRÜNTÜLEME UYGULAMALARINDA KULLANILAN ÇGÇÇ DİZİLERİNİN PERFORMANSINDA ELEMAN RADYASYON DÜZENİNİN ETKİSİNİN ANALİZİ

Altuntaş, Fırat
Yüksek Lisans, Elektrik ve Elektronik Mühendisliği
Tez Yöneticisi: Doç. Dr. Lale Alatan

Eylül 2020, 69 sayfa

Teknolojilerdeki gelişmelerle birlikte, sistemlerin karmaşıklığı da artma eğilimindedir. Sonuç olarak, bu tür karmaşık sistemlerdeki tüm etkileri hesaba katan titiz modeller çok zaman alıcı hale gelir. Bu çalışmada ultra geniş bant (UGB) çok-girişli çok-çıkışlı (ÇGÇÇ) görüntüleme sistemi ele alınmış ve bu tür sistemlerin analizinde kullanılan titiz modellerle elde edilen sonuçlara yakın sonuçlar elde etme çabasıyla basit bir model geliştirilmiştir. Basit veya titiz modeller belirli bir hedef bir gönderici antenle aydınlatıldığında bir alıcı tarafından alınan verileri simüle eder. Tüm gönderici alıcı çiftleri için bu verileri elde ettikten sonra geri projeksiyon yöntemi kullanılarak sistemin nokta dağılım fonksiyonu elde edilebilir. Geliştirilen basit modelin düzgün çalıştığını doğrulamak için ultra geniş bant sinyal özellikleri ve dizi açıklığındaki anten konfigürasyonu analiz edilmiş ve sonuçlar literatürde bulunanlarla karşılaştırılmıştır. Geliştirilen basit modelin düzgün çalıştığını doğruladıktan sonra anten ışıma paterni hesaplamalara eklenmiş ve geliştirilmiş bir model elde edilmiştir. İyileştirilmiş ve titiz modellerden oluşturulan veriler kullanılarak elde edilen nokta yayılım fonksiyonları karşılaştırılarak eleman ışıma paterninin çok-girişli çok-çıkışlı (ÇGÇÇ)

görüntüleme sistemi üzerindeki etkisi incelenmiştir. Bu tezde titiz modelin verilerini oluşturmak için tam dalga elektromanyetik simulasyon yazılımı CST Studio kullanılmıştır.

Anahtar Kelimeler: ÇGÇÇ, Ultra Geniş Bant, Geri Projeksiyon, Nokta Dağılım Fonksiyonu,

To my beloved family

ACKNOWLEDGMENTS

In the first place, I would like to express my deepest gratitude to my supervisor Assoc. Prof. Dr. Lale Alatan for always supporting and guiding me throughout my research. She always made allowance to my endless questions. I never felt alone during my studies under her supervision.

I would like to thank to my colleagues Nihan Öznazlı, Emrah Koç and Remzi Köksal for their support. They provided me assurance that I can discuss any issue with them.

I would like to appreciate ASELSAN for sharing data and experience from their research and development project.

Last but not least, I would like to express my gratitude to my parents for their absolute love and my sister for teaching me to endavour and becoming a torch lighting my path.

I am thankful for the Scientific and Technological Research Council of Turkey and TÜBİTAK 2210-A National Scholarship Program for supporting me in my graduate studies.

TABLE OF CONTENTS

LIST OF TABLES

TABLES

LIST OF FIGURES

FIGURES

LIST OF ABBREVIATIONS

ABBREVIATIONS	
UWB	ultra-wide band
PSF	point spread function
MIMO	multi input multi output

CHAPTER 1

INTRODUCTION

As society advances, demands of the technology increase. In addition to providing a system that is capable of executing a specified task, requirements such as cost effectiveness and viability of the system should also be considered. Although system requirements could be met by theoretical calculations, there would always be practical factors that distort the performance. In order to optimize the system in terms of performance and feasibility, practical issues need to be taken into account during the design process. Since implementation of the physical system in a rigorous way would require devotion of time and resources, development of alternative methods to verify the performance of the designed system come into prominence. In this thesis multi-input multi-output (MIMO) ultra-wide band (UWB) imaging radar is the considered technology and thesis work is focused on the performance analysis of the MIMO array configuration. Generally to make the analysis simple and efficient, array elements are assumed to be isotropic sources radiating in the absence of other array elements and multiple reflections from the target are ignored. As expected, simple model do not provide the most accurate results due to these assumptions. When accuracy is needed full-wave electromagnetic simulation softwares, which take into account every practical issue related with the radar system, are used. As it is well-known, the cost of better accuracy offered by full-wave simulations is the increase in computation time. Therefore the aim of this study is to explore the possibility of improving the accuracy of the simple model by incorporating the radiation pattern of the array elements. If such an improvement can be achieved, then more accurate analysis of the array performance will be possible without losing from computational efficiency.

As radar term is used, the primary applications coming into mind is transmitting radio waves and tracking or detection of objects by collecting reflected signals from targets. By processing the received data, size, location and speed of the targets could be determined. Such systems are to be referred as conventional radar applications operating for surveillance purposes. One of the methods used in conventional radars is the phased array technique. In phased array systems, beam is formed by activating all of the transmitter or receiver antennas at the same time. The reason of simultaneous activation of the elements is to focus the main beam to a desired direction and to increase the operational range by coherent addition of the power from each array element. Associated with the advancements in electromagnetics and microwave systems, radar technique is adapted for different applications. For instance, in imaging radars, surroundings could be mapped by analyzing the scattered waves. Different from surveillance aim in conventional radar, the principal goal of imaging radar is taking advantage of reflectivity of objects and creating 2-D or 3-D images of environment.

In antenna arrays that utilize narrow band signals, emitted electromagnetic waves spatially interfere. Therefore, grating lobes may be observed if the distance between array elements is not chosen properly. This distance restriction varies with the scan angle of the array and it can be at most one wavelength for a broadside array and reduces to half wavelength for an endfire array. Hence to be on the safe side, the spacing between elements should not exceed half of the wavelength in order to prevent grating lobes. Since grating lobes or increased side lobe levels could degrade the dynamic range of view and reduce the image quality, regard should be paid to array element spacing limit and this imposes a restriction on the number of antennas in the array [1]. In imaging radars, the size of the array aperture is generally chosen according to the cross range resolution, δ_{cr}, which is inversely proportional to the size of the aperture, L, as expressed in the following equation:

$$\delta_{cr} = \frac{R}{L}\lambda_c \tag{1.1}$$

where R is the perpendicular distance of the target to the array (down range) and λ_c is the wavelength corresponding to the center frequency. As seen from (1.1), improving the resolution while keeping the distance constant could be achieved by either increasing the operating frequency or size of the aperture. Therefore, providing fine cross resolution at a certain distance might require electrically large aperture and consequently large number of array elements. For instance, achieving 1 cm cross resolution at 0.5m down range which is desired by different applications, length of the horizontal and vertical dimensions of the aperture needs to be 50 times of the wavelength**.** In order to prevent grating lobe in a conventional array system, spacing between antenna elements should not exceed half of the wavelength. As a result, 101 x 101 elements are required to fill the aperture. Such a system would be impractical in terms of antenna number, cost and system complexity. Therefore, different methods specialized for such applications should be considered.

In order to reduce the number of antennas in the aperture, half wavelength spacing rule between elements needs to be violated. That is, sparse arrays would be used. To prevent grating lobes in sparse array, aperiodic structures are used and different thinning methods are proposed in the literature [2]-[5]. Nevertheless, the energy emerging from the prevention of grating lobes would distribute to the side lobes and increase their levels. Even though reduction of number of elements in the system is inspiring, increment of the side lobe level would reduce the resolution quality since array gain would decrease [6]**.**

To overcome the problems of array thinning and sparse array, all parameters of the system should be inspected and fundamental changes need to be made. In [7], effects of UWB signals and short duration pulses on system performance are investigated. When an array operating in a narrow band is considered, signals transmitted from two antennas interfere at every point in space. However in an array operating within an UWB, as shown in Figure 1.1, due to the short durations of the pulses, signals transmitted by two antennas interfere only in a specific region, called interference region (IR). IR for two antennas is determined by the

distance between the elements, d, the duration of the pulse, T, and the down range, R. Two signals transmitted from two antennas interfere as long as the path difference between each antenna to the observation point is less than cT where c is the speed of light. Outside IR, called non-interfering region (NIR), the pulses transmitted from two antennas do not interfere since they cannot exist in that region simultaneously [7]**.** As a result, by utilizing UWB signals in a sparse array configuration, the locations of array elements can be optimized to shift grating lobes into NIR and to reduce the side lobe levels. Application examples of UWB signals in microwave imaging systems can be found in [8]-[11].

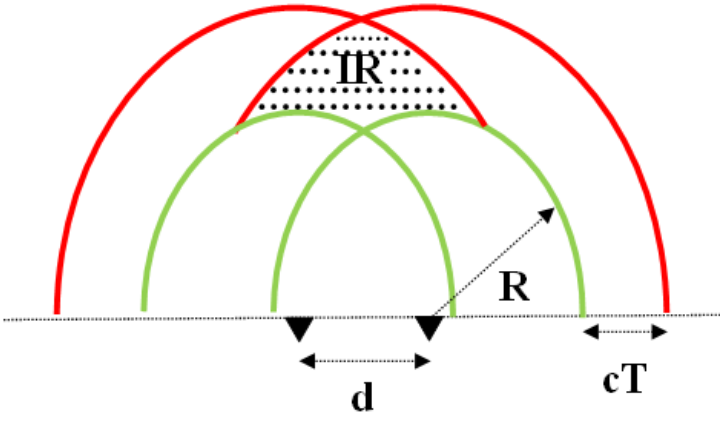

Figure 1.1 Demonstration of IR region

One more degree of freedom can be introduced to the optimization of array element locations by MIMO array configurations. In a MIMO array, each transmitter antenna operates individually and measurements corresponding to all transmitter-receiver pairs are recorded separately as opposed to simultaneous operation of transmitter and receiver antennas in a phased array. In a two-way communication system the two-way radiation pattern is the product of the radiation patterns for the transmitter and receiver arrays. If the same phased array is used for transmitting and receiving, then only one array needs to be optimized. However for a MIMO array, the locations of transmitter and receiver antennas are different and this provides a flexibility in the optimization of two-way radiation pattern. In addition

to this flexibility in the design process, MIMO array configurations are preferred in a wide range of imaging applications [12]-[14] due to independency of the signals offered by the individual operation of transmitters and due to diversity obtained by measuring the scattered fields from the target at multiple locations on the array aperture.

Some performance parameters of a uniformly spaced array, such as beamwidth and sidelobe level, can be predicted from the number, spacing and excitation amplitudes of the elements. However, for a MIMO array such estimation is not straightforward since there exists two arrays (transmitter and receiver) and the two-way radiation pattern needs to be obtained. In order to ease the analysis of MIMO arrays, virtual aperture concept is proposed [15]. Virtual aperture concept is based on the fact that the far-field radiation pattern of an array is the Fourier transform of the aperture field distribution. Recalling that two-way radiation pattern is the product of the radiation patterns for the transmitter and receiver arrays and by using the properties of Fourier transform, virtual aperture of a MIMO configuration could be obtained by taking spatial convolution of transmitter and receiver arrays. As a result virtual aperture can be found by:

$$\nu(r) = T_x(r_t) * R_x(r_r) \tag{1.2}$$

where $\nu(r)$ is the location of the elements in the virtual aperture, * denotes convolution operation, $T_x(r_t)$ and $R_x(r_r)$ are the locations of transmitter and receiver antennas, respectively. Due to the convolution operation, an array that performs transmission and reception in the same aperture would have a larger virtual aperture which is one of the advantages of MIMO systems. With the utilization of ultra-wide band signals and MIMO topology, desired image resolutions could be achieved with practical systems having reasonable number of array elements and aperture size.

As discussed before, the choice of element locations in the transmitter and receiver arrays are vital to prevent grating lobes and to reduce sidelobe levels. The distribution of the elements in the virtual aperture provides an intuition whether

they are placed properly or not. The virtual aperture can be evaluated in terms of redundancy and shadowing. Redundancy occurs when two virtual elements appear to be at the same location. When two virtual elements are at the same location, it means that they will provide same information, so one of them is redundant. Therefore if the number of elements in the virtual array with distinct locations is equal to the product of transmitter and receiver antennas, one may conclude that redundancy is avoided. Since close elements will also provide similar information, uniform distribution of the elements would be optimum in terms of redundancy. On the other hand shadowing can be analyzed by considering a specific cut on the virtual aperture. When the projection of the elements on this cut is investigated, if the projections of two antennas coincide, then this means that one of the elements is shadowed by the other one. As a result, sidelobe level increases in the plane corresponding to this cut. Hence periodic placement of array elements suffers from increased sidelobe levels in the planes possessing periodicity due to shadowing. Shadowing concept will be demonstrated with examples in Chapter 3. Based on redundancy and shadowing concepts, an array configuration is proposed in [16] that achieves better sidelobe level performance in every plane compared to other MIMO configurations that are widely used in the literature. But of course this configuration may not be optimum and other configurations with better performance can be found. Searching the best array configuration, requires the analysis of a MIMO array for every iteration of the optimization algorithm. An accurate and efficient analysis tool is very important for the successful and efficient optimization of the array. For imaging applications the metric for evaluating the performance of the MIMO array is the point spread function (PSF) which corresponds to the image obtained from a point scatterer. The resolution of the radar can be calculated from the slope of the image at the peak location and the sidelobe levels can be concluded by observing the image outside the point scatterer region. To compute the PSF an image reconstruction method is needed. Back projection [17], Kirchhoff migration [18] and range migration [19], [20] are the most frequently used image reconstruction methods in microwave imaging radars.

Due to its simplicity and versatility, back projection method is used in this thesis. An image reconstruction algorithm of a MIMO system takes the measured signals (either time or frequency domain) for every transmitter-receiver pair as input and returns the 3D image in a specified volume as the output. To predict PSF for a given target and a specific array configuration, the measured signals for each transmitter receiver pair needs to be modelled. As discussed at the beginning of this chapter a simple model that considers isotropic sources and ignores multiple reflections from the target, and a full-wave electromagnetic simulator based rigorous model that takes into account of all practical issues are available. Even though rigorous models provide accurate results especially for complex systems which are hard to analyze with simple models, the necessary calculations of such simulations are not easy to handle. Number and structure of antennas, size of the array aperture, shape and size of the target and number of time/frequency samples would increase the work load. For example, point spread function of 17 targets at a certain down range is demonstrated Figure 1.2. This PSF is obtained by using the data acquired from commercially available full-wave electromagnetic simulation software CST Studio. The MIMO aperture comprises 32 transmitter and 32 receiver antennas. Vivaldi antennas are designed as array elements and they are modelled in the simulation environment. The simulation frequency band consists of 1001 points equally sampling the 3-10 GHz with 7 MHz steps. In addition, the simulation needs to be repeated 32 times since transmitter antennas operate one at a time in MIMO systems. As electrical size of the environment, frequency samples and number of antennas are considered, expected execution time of the simulation is in the order of weeks.

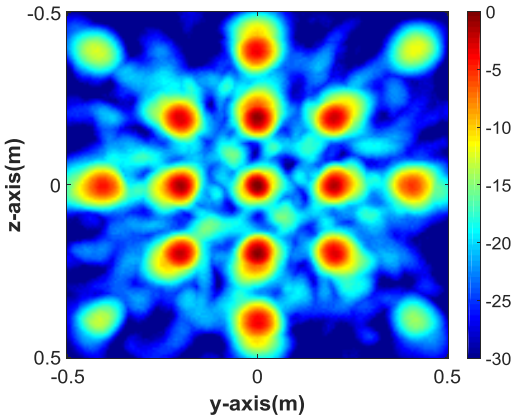

Figure 1.2 Point spread function obtained by data from CST simulation software

In order to analyze the system in a more time efficient way, generally a simple model is used during the design phase of the MIMO array and only small modifications or fine tuning of the array configuration is done based on the rigorous model. In Figure 1.3, point spread function, obtained by using the data generated by the simple model, is presented. As PSF results obtained by rigorous and simple model are compared, it is seen that there exists a lot of differences. For instance, sidelobe levels are different. Moreover, targets outside the center region is less visible in rigorous model. Also, shape of the further targets are different. The aim of this thesis is to explore whether it is possible to improve the accuracy of simple model by incorporating the radiation pattern information of the array elements. If an accuracy improvement can be achieved, the array designed by using this model would need less fine tuning by using rigorous model.

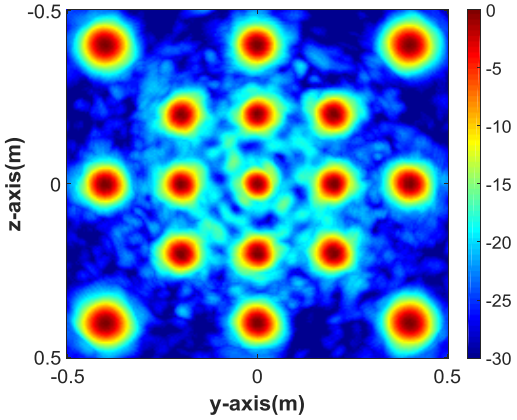

Figure 1.3 Point spread function obtained by data generated through simple model

In addition to that, radiation pattern of the elements are used in back projection algorithm to investigate if the image quality could be improved or not. In the real system, back projection algorithm works with the measured signals. However these signals are attenuated differently for different receiver-transmitter pairs due to the radiation pattern of the antennas. Hence, before passing into the back projection algorithm, measured signals are normalized according to their corresponding two way radiation pattern factors.

In Chapter 2, different aspects of an UWB MIMO imaging system such as UWB signal generation, back projection algorithm, assumptions of the simple model and calibration of the rigorously acquired data are introduced. In Chapter 3, first by using back projection method, point spread functions of widely used MIMO array topologies are computed and their performances are compared. Then the effects of the parameters such as the center frequency, operational bandwidth and aperture size on the performance of the system are investigated. Chapter 4 starts with the comparison of the images obtained by using simple model and rigorous model. Then the formulation to incorporate the radiation pattern into the simple model is presented and the accuracy of this improved model is discussed by comparing to the results obtained by simple and rigorous models. In Chapter 5, effect of the radiation pattern is removed from the measured signals before applying back

projection algorithm and the corresponding results are presented. Chapter 6 concludes the thesis.

CHAPTER 2

IMAGE RECONSTRUCTION IN MIMO ARRAY SYSTEMS

In this chapter of the thesis, different aspects of image reconstruction in MIMO array systems are explained in detail. First, back projection method is introduced which is a widely used image reconstruction algorithm that operates with the data obtained from the MIMO system. For simulations it is necessary to construct an environment and generate this data for a given array configuration and target. Therefore, a simple model and a rigorous model are defined for comparison. Initial definitions and assumptions of simple model characteristics are important in terms of data generation. As long as data generation is compatible with assumptions on simple model, developments and modifications on the model could be made so that we could compare improved model and rigorous model in the later sections of the study. In addition to fundamentals of back projection and simple model characteristics, vitality and significance of calibration process while operating on rigorous model data are expressed.

2.1 Back Projection Method

The main purpose of imaging systems is to analyze the obtained data and reconstruct the image of surroundings. In order to apply the back projection algorithm, configuration of the array elements should be known since distances between antennas and a point in the imaging volume directly affect the phase information of the received signals.

In Figure 2.1, representative demonstration of the MIMO aperture and desired imaging volume are shown. Initially, distances between antennas and imaging volume should be calculated. In Figure 2.1, aperture includes both transmitter and

receiver elements where they are represented as t_i andr_j, respectively. On the other hand, imaging volume is meshed into small pieces defined as vortex and denoted by p_k.

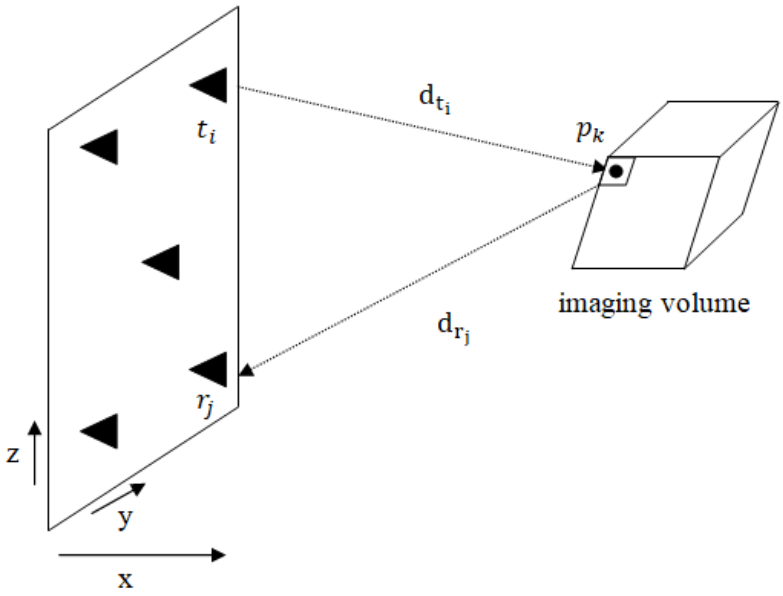

Figure 2.1 Illustration of signal path

Distances between each vortex in the imaging volume and antenna elements are calculated by using the equations:

$$d_t(t_i, p_k) = \sqrt{\left(x_{p_k} - x_{t_i}\right)^2 + \left(y_{p_k} - y_{t_i}\right)^2 + \left(z_{p_k} - z_{t_i}\right)^2}$$

$$d_r(r_j, p_k) = \sqrt{\left(x_{p_k} - x_{r_k}\right)^2 + \left(y_{p_k} - y_{r_j}\right)^2 + \left(z_{p_k} - z_{r_j}\right)^2} \quad (2.1)$$

where $d_t(t_i, p_k)$ and $d_r(r_j, p_k)$ are distances of i^{th} transmitter and j^{th} receiver to k^{th} imaging point.

The signal received by r_j due to the wave transmitted by t_i, can be measured in time or frequency domain. Back projection algorithm could be applied also either

in time or frequency domain. In [21], computation cost of back projection method in time domain and different methods in frequency domain are compared. Since the implementation of the back projection method in time domain is computationally more efficient, the formulation will be presented for time domain. If the data corresponding to (t_i,r_j) pair is measured in frequency domain, $\mathrm{U}(\mathrm{t_i}, \mathrm{r_j}, \mathrm{f})$, it can be transformed to time domain, $\mathrm{u}(\mathrm{t_i}, \mathrm{r_j}, \mathrm{t})$, by using the following Fourier Transform relation:

$$\mathrm{u}(\mathrm{t_i}, \mathrm{r_j}, \mathrm{t}) = \mathrm{F}^{-1}(\,\mathrm{U}(\mathrm{t_i}, \mathrm{r_j}, \mathrm{f})\,) \tag{2.2}$$

It should be noted that in addition to the fields scattered from the target, direct field emitted by the transmitter antenna will be received by the receiver antenna as shown in Figure 2.2. Back projection method assumes that the direct fields are eliminated from the measured signal either by using time gating (direct and reflected fields arrive at different times due to the path difference) or by using a calibration method as discussed at the end of this chapter. As a result measured signal contains only the scattered field information.

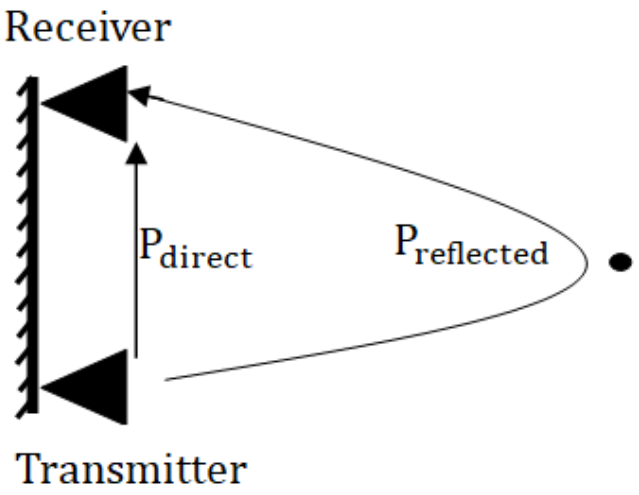

Figure 2.2 Illustration of direct and reflected signals

The main idea of the back projection algorithm is to back propagate the signals transmitted from and received on the array aperture plane to the desired vortex in

the imaging volume. Back propagation means compensating for the time delay due to the propagation of electromagnetic waves. Since locations of antenna elements and desired imaging vortex are known spatially, an advance function could be calculated as:

$$\varsigma(t_i, r_j, p_k) = \frac{d_t(t_i,p_k) + d_r(r_j,p_k)}{c} \tag{2.3}$$

where $\varsigma(t_i, r_j, p_k)$ gives the calculated total travel duration between respective antenna elements and desired imaging vortex while c is simply the speed of light. Back projected signal of a transmitter and receiver pair is calculated by:

$$u_{bp} = u(t_i, r_j, \varsigma)\, d_t(t_i, p_k)\, d_r(r_j, p_k) \tag{2.4}$$

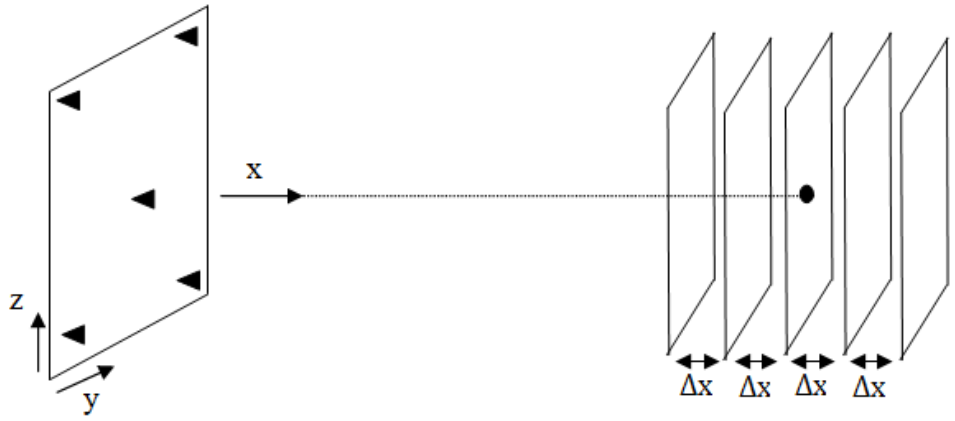

Figure 2.3 Representation of different layers in down range

Note that spherical wave propagation $\left(\frac{e^{-jkr}}{r}\right)$ is assumed to be able to apply the analysis to near field imaging systems as well. The image function at p_k, $m(p_k)$, can be calculated through a summation over all possible transmitter and receiver antenna pairs as:

$$m(p_k) = \sum_{t_i} \sum_{r_j} u_{bp} \tag{2.5}$$

At the end of back propagation algorithm a three dimensional (3D) image is formed. However in general for better visualization, two dimensional (2D) images are preferred and as shown in Figure 2.3, 2D images on planes parallel to the array aperture are used. Different approaches can be used to transform the 3D image into 2D. Three different representations are used in this thesis. The first one is denoted as "normal" where the image at a specific plane ($X=X_0$) is considered only. For targets extending in down range direction, 2D image at several constant x surfaces need to be observed. To better visualize the 3D image, for a specific (Y,Z) coordinate, maximum value over all X coordinates are plotted in most of the imaging applications. This type of 2D plot will be denoted as "max". The main purpose of taking the maximum in down range could be called as a filter. Even though image function peaks at target locations, due to the time duration of the signals, image function does not drop drastically. By observing image function in down range and taking the maximum value, image function is to be localized around the targets. Therefore, side lobe level around the targets is expected to decrease. Yet, finding the maximum value in the down range might cause problems. In some scenarios considering the system parameters such as array topology, target placements and operating bandwidth, there might be spikes as a result of back projection in the down range. In case of maximum point spread function utilization, false images might emerge or delusion in terms of size and location of the actual target. Therefore another representation is also widely used in which the value at a specific (Y, Z) coordinate is the summation of the values on a number of planes in the neighborhood of the target in the down range. This representation is denoted by "summation". The advantage of summation representation is having less tendency to encounter spiky results that might create problems in maximum representation. The reason is that summation is a smoothing operator that decreases the effect of possible exceptional results in down range due to the accumulation of different layers. However, there would be a disadvantage for this representation. Since all values are summed up, it is accepted that side lobe level would be higher than other representations.

In order to evaluate the performance of a MIMO array imaging system, point spread function (PSF) is used. PSF is the image obtained by using a point scatterer. The sharpness of the peak at the target location indicates the resolution of the system and the level of local maximums outside the target region indicates the sidelobe level of the system. The number of point scatterers can be increased and they can be distributed to the imaging volume to observe the performance of the array at different locations in the imaging volume. In order to obtain PSF by using back propagation algorithm, the signal measured by each transmitter-receiver pair need to be simulated for a given array configuration and system parameters. In the next section a simple model to generate this data will be presented.

2.2 MIMO Array Data Generation with Simple Model

In this part of the work, the simple model used to simulate the data measured by the MIMO array will be constructed together with the assumptions made to simplify the problem. Different methods used to transform the frequency domain transmitted signal into the time domain will be introduced in the following section.

2.2.1 Generation of Transmitted Signal

One of the reasons of frequency domain data usage is that frequency based devices are used in practical measurements. For instance, the main microwave measurement tool is the vector analyzer which gives the frequency response of the system. Therefore, signal would be defined and data would be generated in frequency domain so that the simple model could be comparable with a rigorous model that is used in electromagnetic simulation software or practical measurements. In other words, possible discrepancy which might be caused by data transformation is prevented.

Even though there are multiple methods to construct an ultra-wide band signal, utility and simplicity of the signal definition is important. Since the work load is

directly proportional to the predefined parameters such as number of transmitter and receiver antennas, targets, number of frequency samples, their effect on process cannot be changed. Therefore, signal definition procedure has a huge impact on the time required to complete simulations.

The frequency samples of the data is available only for positive frequencies but before applying inverse Fourier transform the signal needs to be extended to negative frequencies. The first method for this extension is the most fundamental one in which complex conjugate of the positive side is considered for the negative side as shown in Figure 2.4. After inverse Fourier transform, the resulting signal in time domain is a modulated signal.

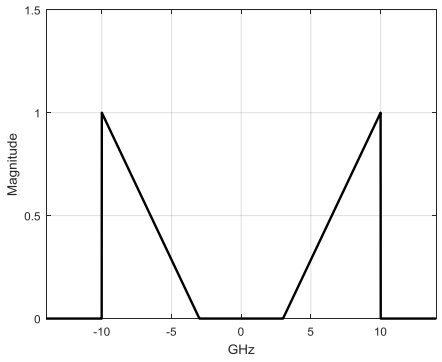

Figure 2.4 Frequency domain signal definition using method I

The envelope of the modulated signal carries the necessary information, so the second method is based on this observation. In the second method first the positive side is shifted to baseband to eliminate the modulation, and then its complex conjugate is defined for the negative side as shown in Figure 2.5.

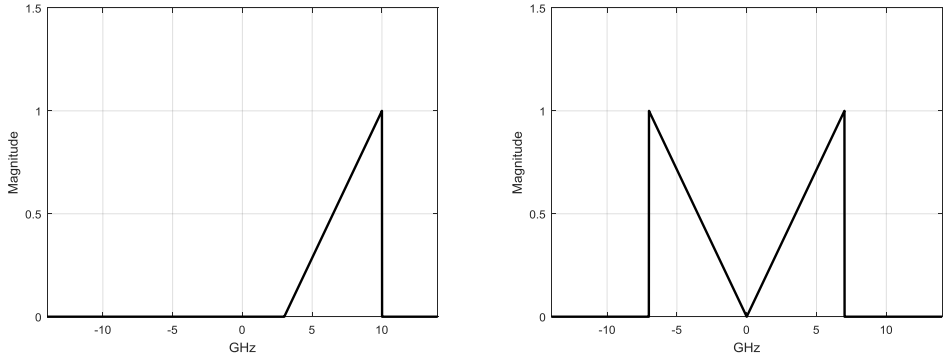

(a) (b)

Figure 2.5 Frequency domain signal definition using method II (a) measured signal (b) shifting to baseband and generation of complex conjugate in the negative side

In the third method, complex envelope of the modulated signal is used. The signal is only shifted to origin as shown in Figure 2.6. Since the frequency domain signal is not symmetric with respect to origin, the corresponding time domain signal will be complex. Even though a complex time domain signal is not practically possible and meaningful, it provides results as accurate as the first and second method [22]. For the sake of simplicity, this method is utilized in this study.

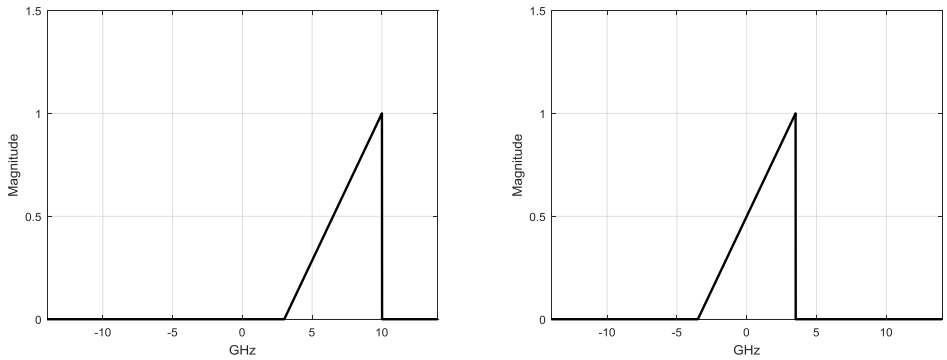

(a) (b)

Figure 2.6 Frequency domain signal definition using method III (a) measured signal (b) shifting to origin

2.2.2 Simple Model

As illustrated in Figure 2.7, there is a MIMO array with known antenna number and locations, there is a point scatterer at a given location and a wave is emitted from one of the transmitter antennas, the scattered signal received by one of the receiver antennas need to be computed.

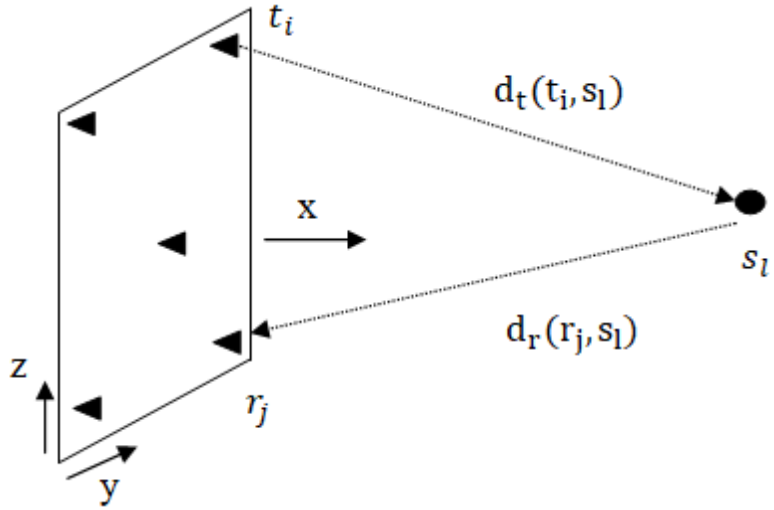

Figure 2.7 Forward problem for a point scatterer

Some assumptions are made to simplify the analysis. These assumptions are summarized as:

1. Antennas are assumed to be isotropic for every frequency.

The prime requirement that an antenna should meet in the system is that effective operating band in which antenna is matched to microwave circuitry supports the ultra wide band signal. Even if the antenna operates in such a bandwidth, its performance would change depending on the frequency. For example, radiated power would differ according to the frequency, moreover, response of each antenna in the array show differences due to the manufacturing effects. Hence, one should not expect to obtain same performance from an antenna at every frequency.

Furthermore, each antenna has a radiation pattern so that the power radiated by the antenna would not be same for all directions. To sum up, in practice, the antenna radiation coefficient depends on frequency and directions but in order to simplify the analysis it will be assumed to be one for all directions and frequencies.

2. The field incident on the point scatterer will be fully reflected.

Regarding the electromagnetic theory, each material has different reflection coefficient, ρ. Hence, received signal level is greatly dependent on the reflected signal. In practice, there would be additional signal loss due to the materials with $\rho < |1|$. In simple model point scatterers will be accepted as perfect electrical conductor with $\rho = -1$.

3. Only single reflection is assumed, multiple reflections are ignored.

In practice, there would be infinite number of reflections from scatterers and antennas. In order to reduce the complexity in the analysis, it is accepted that there would be only single reflection from each target.

Based on the above assumptions, the spherical wave emitted by i^{th} transmitter will arrive to the l^{th} scatterer and reflected with reflection coefficient -1, and then it will be received by the j^{th} receiver antenna with coefficient 1. The total time duration of this travel is expressed as:

$$\tau(t_i, r_j, s_l) = \frac{d_t(t_i,s_l) + d_r(r_j,s_l)}{c} \tag{2.6}$$

After travel times for each transmitter, receiver and target are calculated, the received signal at frequency, f. can be easily written as:

$$U_l(t_i, r_j, f, s_l) = \frac{e^{-j\,2\pi\,f\,\tau(t_i,r_j,s_l)}}{d_t(t_i,s_l)\;\; d_r(r_j,s_l)} \tag{2.7}$$

There might be multiple scatterers. In that case received signal for s number of scatterers can be written as:

$$U(t_i, r_j, f) = \sum_{l=1}^{s} U_l(t_i, r_j, s_l, f) \tag{2.8}$$

The expression in (2.8) is the final form of the synthetically generated frequency domain data which is to be used in back projection algorithm after transforming into time domain.

2.3 Calibration Process for Rigorous Model

Rigorous model refers to the model in which the MIMO array is constructed by using a specific type of array element and received signals in the presence of a target are computed rigorously with the help of full-wave electromagnetic analysis software. Frequency domain solver of CST Studio [23] is utilized in this thesis and Vivaldi antennas are used as array elements. The raw data obtained from simulations is not directly usable in the back projection algorithm. In Figure 2.8, received signal between t_1 and r_1 is demonstrated for a sample case. The received raw data represented as $U_l(t_1, r_1, s_1, f)$ involves additional and unwanted signals. For example, only green signal is desired but there would be direct coupling between antennas, scattering from other antenna elements and reflections from the ground plane that supports the antennas. In order to remove the effects of these unwanted signals, calibration is required.

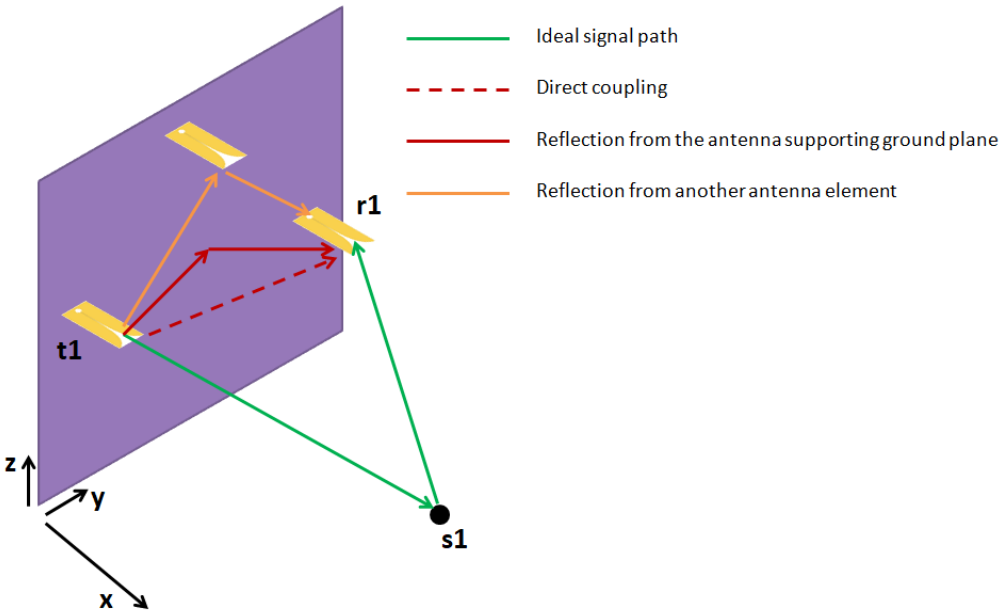

Figure 2.8 Demonstration of rigorous model simulation environment

As discussed before, the signal received by a receiver antenna involves both direct coupled fields from the transmitter and the scattered fields from the target. In addition to direct coupling, there would be unwanted reflections from the MIMO system or surroundings. Since back propagation algorithm assumes that the received signal is only due to the scattering from the target, elimination of undesired signals is necessary. In order to filter out the unwanted signals derived from undesired environmental reflections and direct couplings, it is required to take measurement when there is not any reflective object in the imaging volume. Once the data for empty volume case is obtained, it will be subtracted from the actual measurement that includes information of targets. The calibration is simply expressed as:

$$U_{cal1}(t_i, r_j, f) = U_{measured}(t_i, r_j, f) - U_{empty}(t_i, r_j, f) \quad (2.9)$$

where $U_{measured}$ and U_{empty} are the data obtained from CST software when the target is present and removed, respectively. U_{cal1} represents the calibrated data.

Back propagation algorithm depends on the phase shift information between the transmitted and received signals and it assumes that this phase shift occurs due to propagation of the wave from the aperture of the transmitter antenna to the target, then from the target to aperture of the receiver antenna. But the extra connections between the antenna and the measurement device will introduce extra phase variation. Moreover for UWB antennas like Vivaldi antenna, the phase center of the antenna changes with frequency [24]. Therefore there will be an extra frequency dependent phase variation in the measured data and it needs to be removed. There are several methods to correct this phase error in the MIMO system. In order to estimate this frequency dependent phase variation, a canonical scattering problem is solved with a known scatterer where the reflected fields from this scatterer are known. In this calibration process, generally a conducting sphere or an infinitely large conducting plane is used [25] so that all transmitted waves would reflect. In this study as suggested in [26], an infinitely large conducting plane is used and it is illuminated by a transmitter antenna placed at a distance x from the plane, then the reflected field is measured. To simplify the simulation model in CST, image theory is used. The conducting plane is removed and an identical receiver antenna is placed at a distance $2x$ from the transmitter antenna (as shown in Figure 2.9) and the transfer function between the antennas, S_{21}, is obatained.

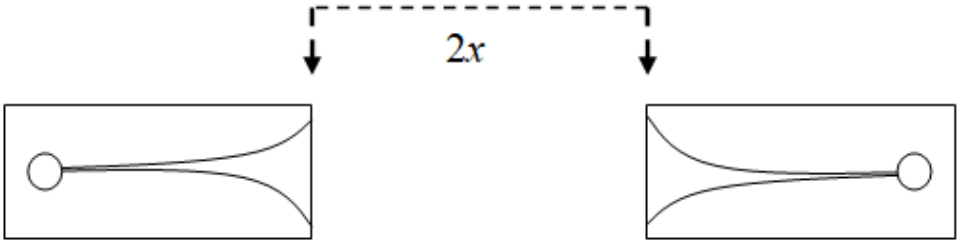

Figure 2.9 CST setup used for phase calibration

When the effect of phase change due to the propagation of waves between transmitter and receiver antennas $\left(e^{\frac{j2\pi f2x}{c}}\right)$ is removed from the transfer function, the remaining part represents the frequency dependent extra phase shift due the variations in the phase center of the antenna and the phase contribution of other components in the measurement setup like feed structure of the antenna. The remainder part is calculated as:

$$H_f(f) = S_{21}(f)e^{\frac{j2\pi f2x}{c}} \tag{2.10}$$

The measured signal should be divided by this remainder term for phase calibration. The resulting calibrated data which is to be utilized in back projection algorithm is simply expressed as:

$$\mathrm{U_{cal2}}(\mathrm{t_i}, \mathrm{r_j}, \mathrm{f}) = \mathrm{U_{cal1}}(\mathrm{t_i}, \mathrm{r_j}, \mathrm{f})/\mathrm{H_f(f)} \tag{2.11}$$

CHAPTER 3

ANALYSIS OF SYSTEM PARAMETERS

Since this work proposes an alternative method to examine the practical MIMO imaging systems without creating complex models, a matlab code is generated to carry out the data generation and back projection operations which are explained in the previous chapter in detail. Before studying the differences between simple and rigorous models, working principle of the generated code needs to be verified by analyzing the fundamentals of MIMO imaging systems.

Initially, different MIMO array configurations are implemented in the generated code and corresponding point spread functions are calculated and compared with results introduced in [16]. Then, effects of center frequency, operating bandwidth and aperture size on image resolution are investigated. That is, simple model is verified by comparing with related works and by examining its compliance with theoretical calculations.

3.1 Effect of MIMO Configuration

Placement of the antennas in the aperture is one of the most determinant factors in the performance of the imaging systems. As mentioned in the previous parts, with the utilization of ultra-wide band signals, $\lambda/2$ antenna spacing restriction can be lifted. Therefore, location of each element needs to be specified attentively. In [16], Zhuge and Yarovoy studied four widely known MIMO configurations and calculated respective point spread functions. In this part, same array topologies are used and point spread functions (PSF) are acquired when a single pointwise scatterer is located in the origin x=0.5m. During the calculation of PSF, frequency domain data in simple model is generated by sampling the 3 - 10 GHz operational bandwidth with 7 MHz steps and back propagation is used for image

reconstruction. In the following figures maximum representation is used to convert 3D PSF information into 2D plot.

3.1.1 Rectangular Array

In the rectangular formation, there exists 9 transmitter and 16 receiver antennas in the aperture as shown in Figure 3.1(a). As seen from the Figure 3.1(b), the virtual aperture is comprised of uniformly distributed elements. Due to the periodicity in element distribution, shadowing effect is expected to be observed along the periodicity directions. As expected, higher side lobe levels are observed in horizontal and vertical planes of PSF which is presented in Figure 3.1(c). Even though uniform virtual element distribution provides fine cross range resolution around the target which is inside the interference region, rectangular array needs to be optimized for a better imaging quality.

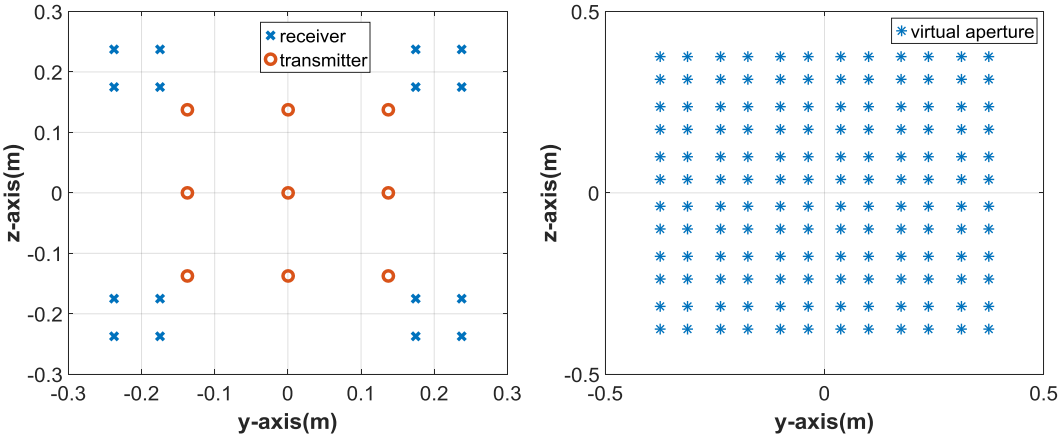

(a) (b)

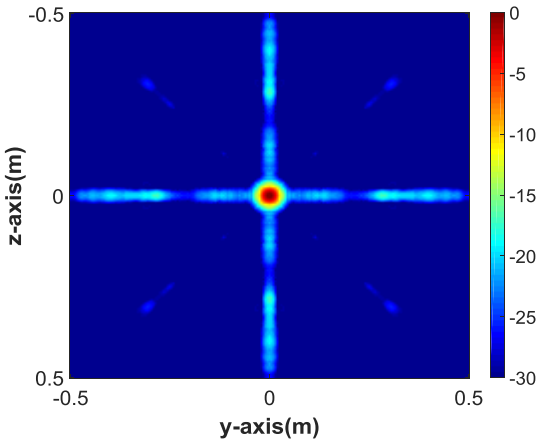

(c)

Figure 3.1 (a) Rectangular array with 16 receivers and 9 transmitters (b) virtual aperture compromised of 144 elements (c) PSF

3.1.2 Mills Cross Array

In the Mills Cross Array configuration, transmitters and receivers are placed on diagonals in the array aperture (Figure 3.2(a)). Even though total number of antennas in the aperture is same as those in the rectangular topology, as seen in Figure 3.2(b), virtual aperture consists of 156 elements which is greater than the number of elements in rectangular topology. Figure 3.2 Mills Cross array demonstrates a uniform coverage in virtual aperture similar to rectangular topology

and it also suffers from shadowing. In Figure 3.2(c), increased side lobe levels can be observed in the diagonal cuts where periodicity exists.

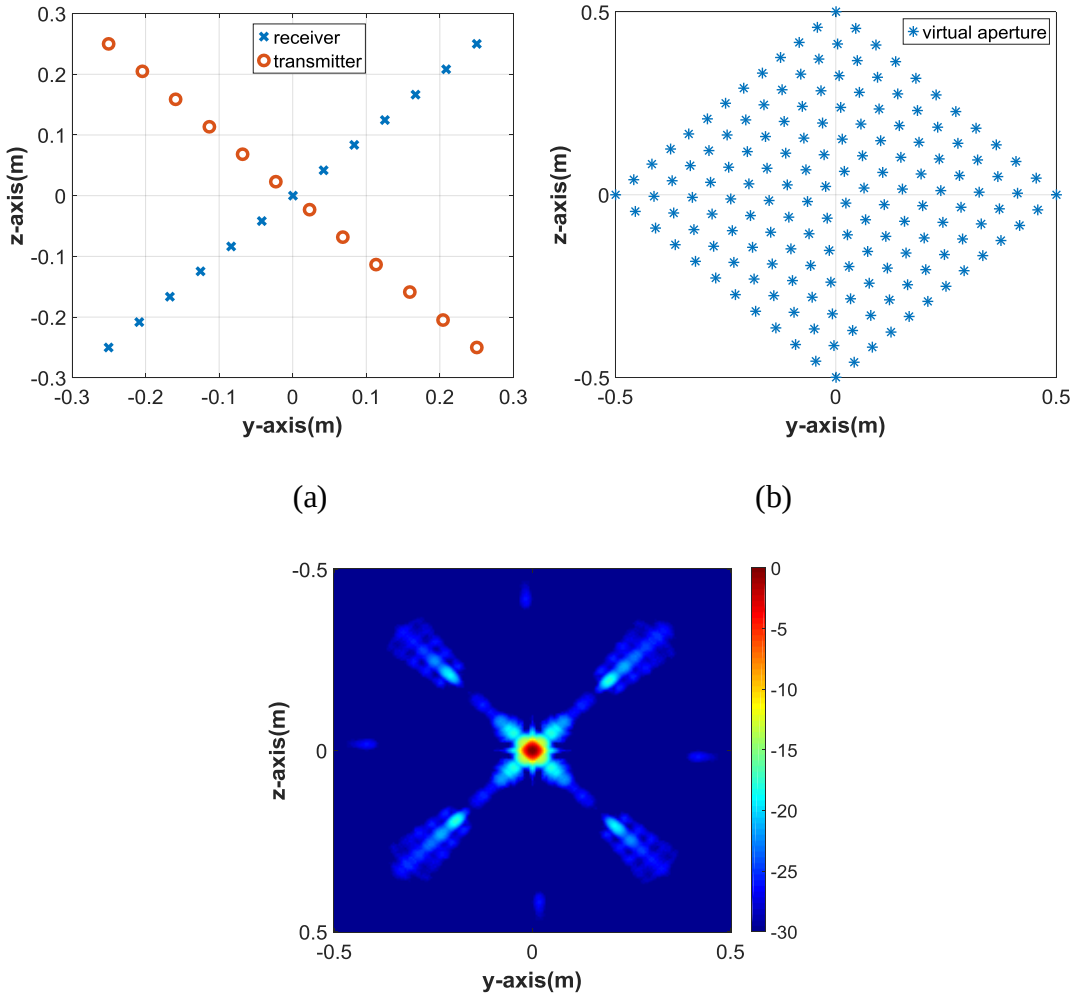

(a) (b)

(c)

Figure 3.2 (a) Mills Cross array with 13 receivers and 12 transmitters (b) virtual aperture compromised of 156 elements (c) PSF

3.1.3 Spiral Array

The main idea of spiral array is to keep effect of shadowing low by avoiding periodicity in antenna placement (Figure 3.3(a)). Different from rectangular and Mills Cross configurations, spiral array does not provide uniform element

distribution in virtual array (Figure 3.3(b)). As a result, high level sidelobes are not concentrated on one or two planes but they are distributed with a lower level as seen in Figure 3.3(c). However it can be also observed from the wider image of the target that resolution is worse compared to rectangular and Mills Cross configurations. This is due to the redundancy caused by the close elements in the virtual aperture. Close elements provide similar information so they don't have any additional contribution. Nevertheless, there exists a tradeoff between reducing sidelobe level low outside the focusing region and cross range resolution.

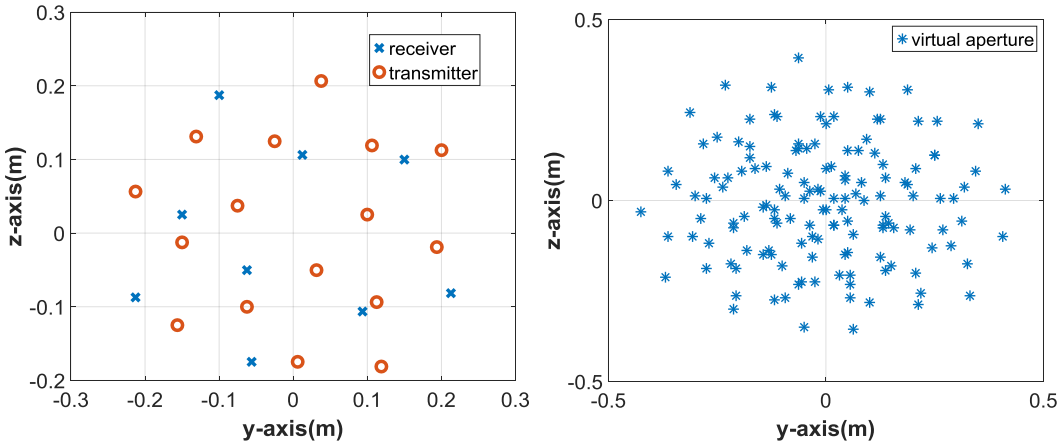

(a) (b)

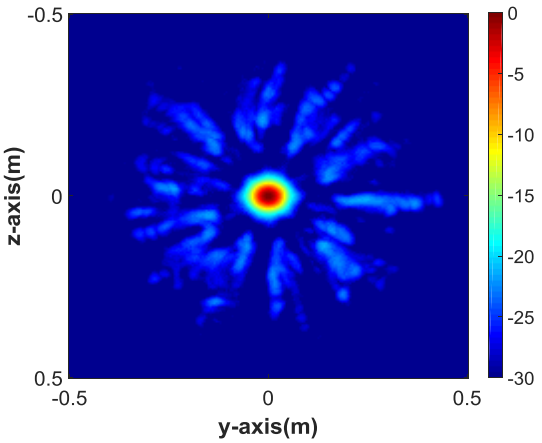

(c)

Figure 3.3 (a) Spiral array with 16 receivers and 9 transmitters (b) virtual aperture compromised of 144 elements (c) PSF

3.1.4 Curvilinear Array

As seen in Figure 3.4(a) curvilinear structure is obtained by placing transmit and receive elements on ring and spiral structures, respectively. By mixing ring and spiral structures, coverage of virtual aperture (Figure 3.4(b)) is improved and a more uniform distribution is obtained compared to spiral only configuration. It should be noted that periodicity is also avoided with this configuration. Consequently, as can be observed from the PSF in Figure 3.4(c), a better cross range resolution and a lower side lobe level outside the focusing region are obtained compared to spiral only configuration.

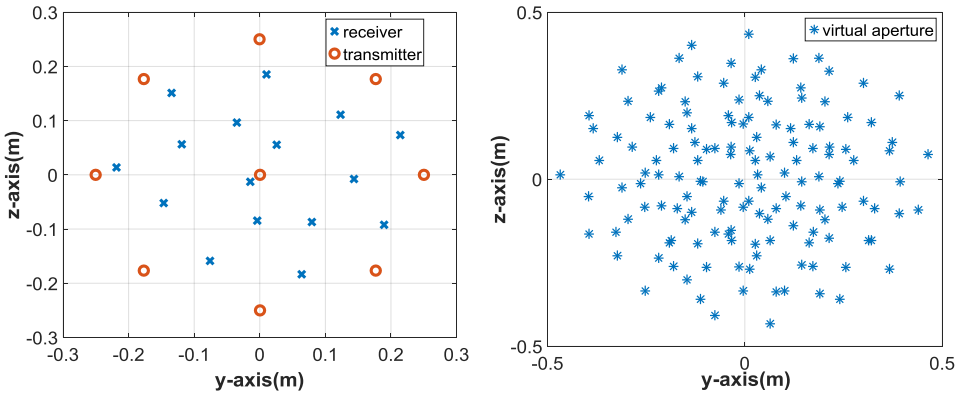

(a) (b)

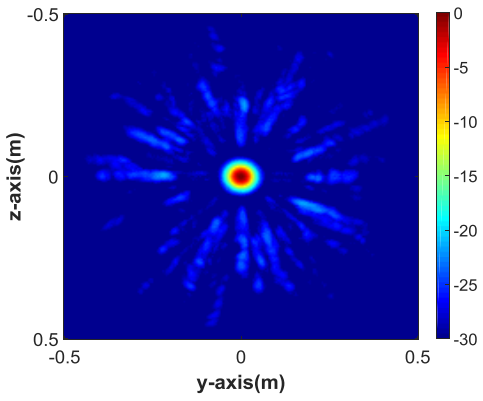

(c)

Figure 3.4 (a) Curvilinear array with 16 receivers and 9 transmitters (b) virtual aperture compromised of 144 elements (c) PSF

3.1.5 Comparison of MIMO Topologies

In order to verify the working principle of the constructed simple model and back projection algorithm, calculated point spread functions for different MIMO arrays are compared with Zhuge and Yarovoy's experiments demonstrated in [15]. From Figure 3.5, it is seen that same MIMO topologies have similar point spread functions even though simple model is utilized in this study on the other hand Zhuge and Yarovoy realized a practical imaging system and conducted the analyses in a rigorous way. For instance, the MIMO arrays are constructed with Vivaldi antennas. Also, measurements are taken with network analyzer by switching between all transmitter and receiver elements regarding the working principle of MIMO system. In addition, system suffers from direct coupling between elements and a calibration method is proposed to eliminate the unwanted signal.

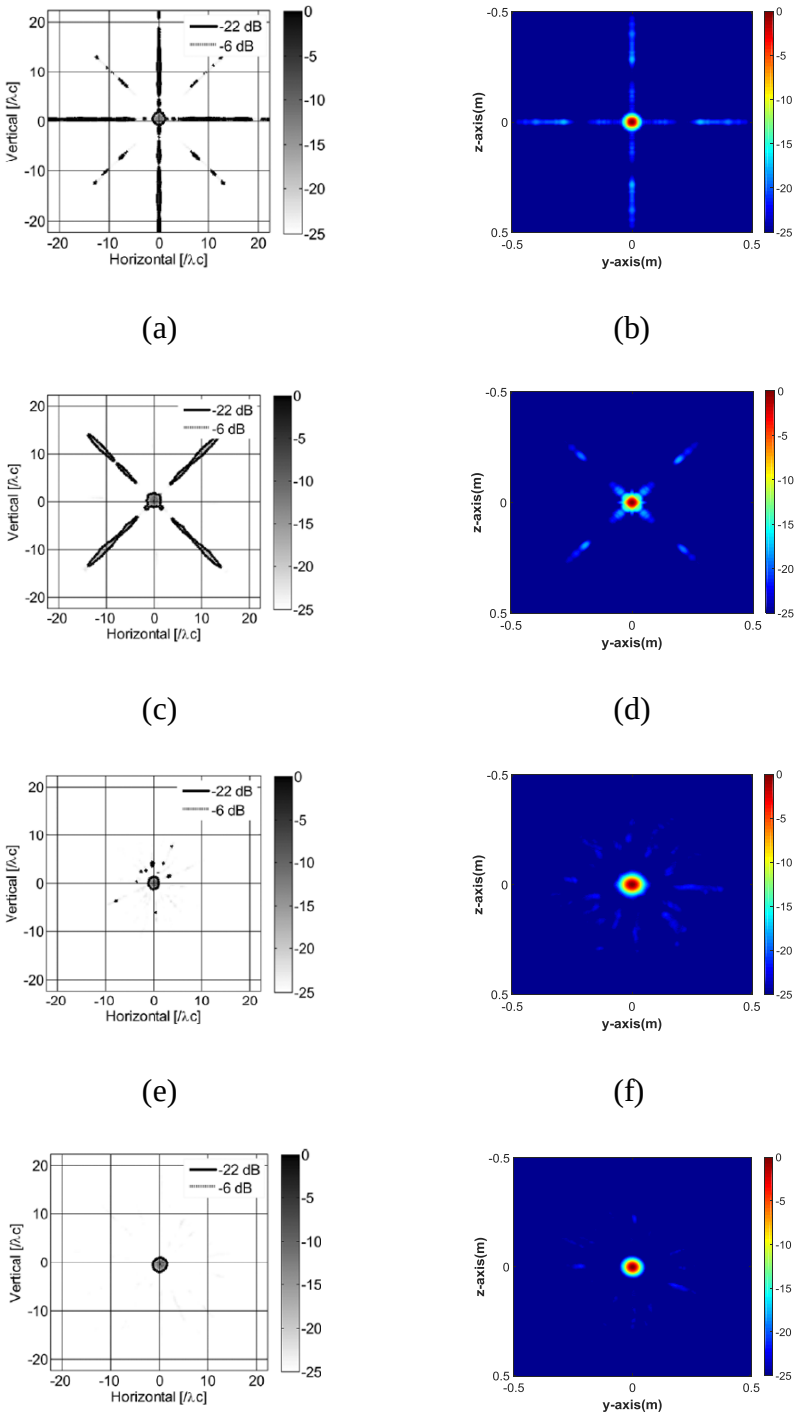

Figure 3.5 Point spread functions for (a) rectangular array from [16] (b) rectangular array from this work (c) Mills cross array from [16] (d) Mills cross array from this work (e) spiral array from [16] (f) spiral array from this work (g) curvilinear array from [16] (h) curvilinear array from this work

3.2 Effect of Signal Characteristics

In order to analyze the working principle of simple model, signal characteristics are changed and their effects on point spread function are analyzed. In the analyses, three different signals given in Table 3.1 are utilized. By comparing signal I and III, effect of bandwidth on cross range resolution is analyzed. Since center frequency of both signals is same, it is expected that cross resolutions should also be same according to $\delta_{cr} = (R/L)\,\lambda_c$. In order to review the results in a more numerical way, cross range resolution is associated with 3-dB locations where peak power is halved. Then, by comparing signal I and II where bandwidth percentages are same, effect of center frequency is inspected.

Table 3.1 Characteristics of different signal types

Signal Type	Center Frequency (GHz)	Bandwidth	Operational Band(GHz)
I	8	50%	6 - 10
II	5.33	50%	4 - 6.67
III	8	100%	4 - 12

During the point spread function calculations, modified spiral array configuration, demonstrated in Figure 3.6(a) is utilized. The array consists of 32 receiver and 32 transmitter antennas with 1024 virtual elements as shown in Figure 3.6(b). The main reason of utilizing this spiral array is that rigorous model measurements, which will be used later, are taken with this MIMO configuration.

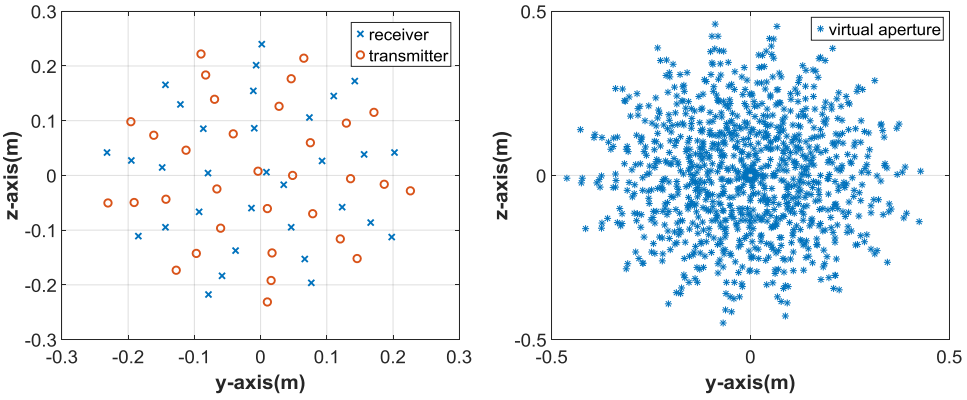

(a) (b)

Figure 3.6 Spiral array with 32 transmitters and 32 receivers (a) antenna configuration (b) virtual aperture compromised of 1024 elements

In Figure 3.7, point spread function of the MIMO configuration defined in Figure 3.6 with signal I is given. In order to better compare the effects of signal characteristics, the PSF along z=0 cut is plotted in Figure 3.8 for positive values of y-axis.

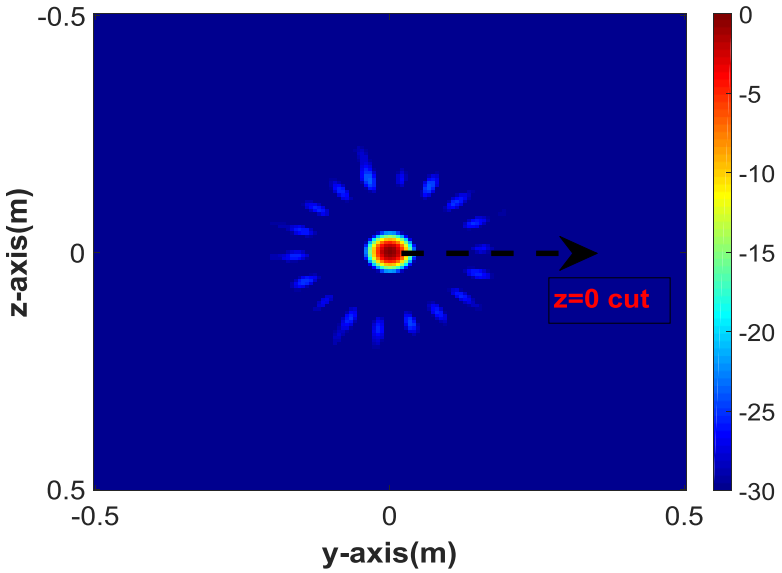

Figure 3.7 Point spread function obtained by the data generated through simple model utilizing signal I

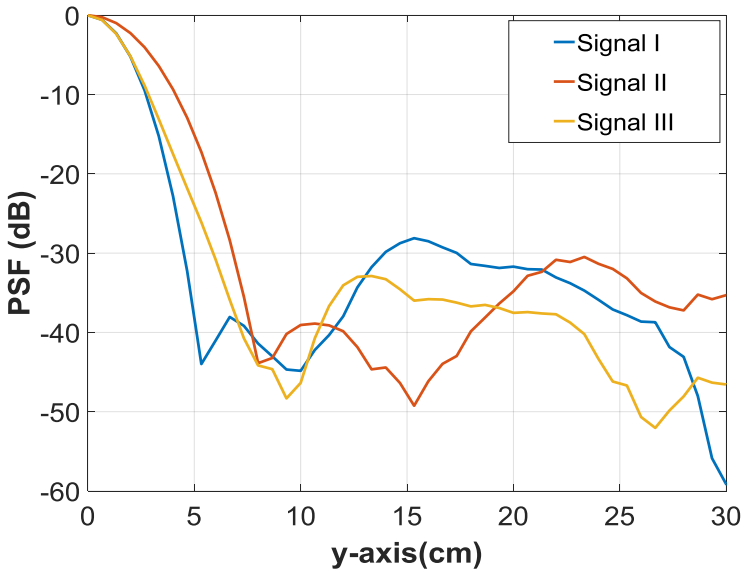

Figure 3.8 Point spread functions for different signal types for z=0

As seen from the Table 3.2, 3-dB locations, which are a measure of resolution, are same for signal I and III due to the fact that signals are generated around same center frequency. On the other hand, lower sidelobe level compared to signal I is observed for signal III, since it has a larger bandwidth. As the bandwidth increases the transmitted pulse becomes narrower and consequently the probability of interference between two antennas gets smaller, so side lobe level decreases.

Table 3.2 Point spread function analyses for different signal types

Signal Type	3-dB Location (cm)	Side Lobe level (dB)
I	1.6	-28.1
II	2.3	-30.5
III	1.6	-32.9

As results of signal I and II are compared, signal I provide better cross range resolution than signal II due to the higher center frequency and they result in similar side lobe levels due to same bandwidth.

3.3 Effect of Aperture Size

Apertures with different physical sizes are compared in this section. Locations of transmitter and receivers are simply scaled in accordance with the aperture enlargement rate. In the Table 3.3, test conditions are expressed.

Table 3.3 Different aperture sizes with same signal characteristics

Aperture Type	Center Frequency(GHZ)	Aperture Size (m)	Operational Band(GHZ)
I	6.5	0.25 x 0.25	3 - 10
II	6.5	0.5 x 0.5	3 - 10

Similar to previous analysis, point spread function is calculated at z=0 cross section for both aperture types as seen in Figure 3.9.

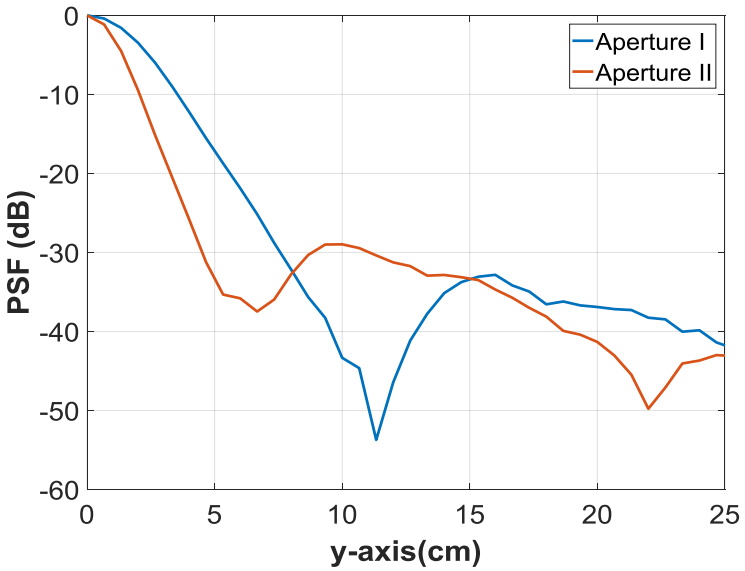

Figure 3.9 Point spread functions for different aperture types at z=0

As seen from the PSF plot in Figure 3.9 and 3-dB locations in Table 3.4, physically larger aperture II provides better cross range resolution as expected. On the other hand sidelobe level is higher for aperture II, which might be due to keeping the

number of elements same while enlarging the aperture. More antenna elements are required to uniformly sample the larger aperture.

Table 3.4 Point spread function analyses for different aperture types

Aperture Type	**3-dB Location (cm)**	**Side Lobe level (dB)**
I	1.8	-32.8
II	1	-29

CHAPTER 4

IMPROVEMENTS ON THE SIMPLE FORWARD MODEL BY USING RADIATION PATTERN OF ARRAY ELEMENTS

In the previous chapter, the fundamental parameters of the MIMO imaging system are studied by analyzing the point spread function of a single target positioned at origin. However the performance of the MIMO imaging system generally differs for targets placed at locations other than the origin. In order to investigate these differences, multiple target scenario is studied in this chapter. 32x32 spiral MIMO array configuration presented in Figure 3.6 is used throughout the analysis in this chapter. 17 point scatterers are placed at a distance of 0.5m from the array aperture with locations shown in Figure 4.1.

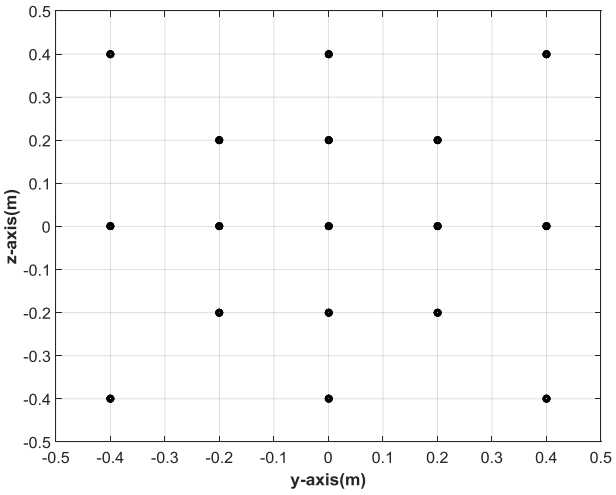

Figure 4.1 Representation of 17 scatterers in yz-plane

First simple model will be used to simulate MIMO array data, then rigorous model data obtained from CST simulations of multiple scatterers under the illumination of Vivaldi antennas, will be utilized. By comparing and pointing out the differences between simple and rigorous models, necessity of modification of simple model

will be explained. Thus, construction of improved model by including simulated radiation pattern of Vivaldi antenna into the simple model will be described. In addition to the point spread function comparisons, time domain analysis are conducted on the received signals in detail to observe differences between models during the data generation process.

4.1 Simple Model

In Chapter 2, three different representation of back projection algorithm are explained. Even though summation and maximum representations require additional calculations in different down ranges which increase the work load, they provide utilization of volumetric imaging and different perspectives to interpret the working principle of model. In Figure 4.2, different representations of point spread functions acquired with MIMO data generated with simple model are given.

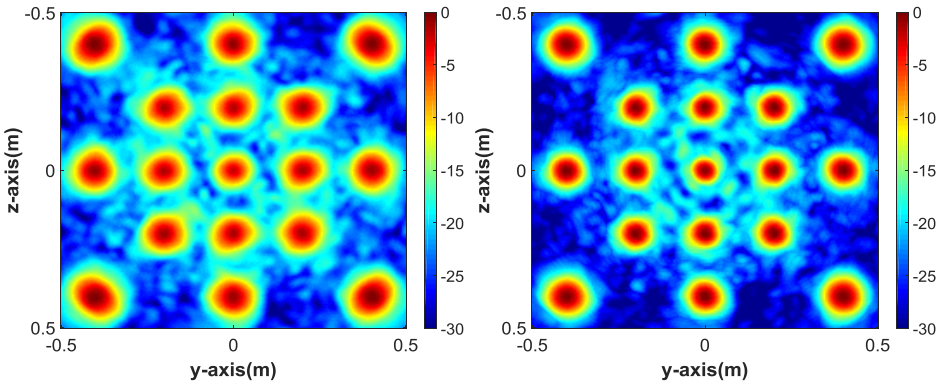

(a) (b)

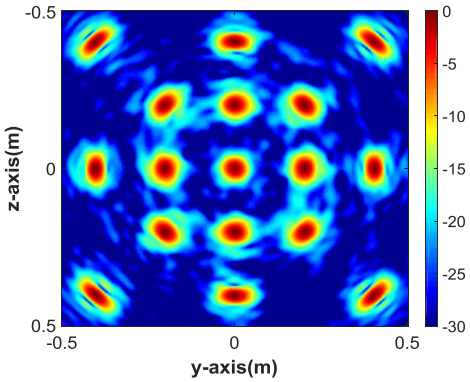

(c)

Figure 4.2 Simple model point spread function with 17 targets located at x=0.5m (a) summation representation (b) maximum representation (c) normal representation

The summation representation, in which planar sections with different down ranges are summed, demonstrates that each target is identifiable. Yet, due to summation, the average signal level is higher than others. In addition to that if targets were located closer, it would be hard to distinguish them explicitly. This type of representation is not preferred.

When normal representation at x=0.5m is analyzed, it can be seen that shape of the objects outside the center region, are distorted. The reason of image deformation at exact down range in which targets are located would be originated from the

focusing region related to the size of aperture. Targets located closely to the origin are inside the focusing region of 0.25 x 0.25m MIMO aperture. As can be observed from the maximum representation, indeed the complete image of the targets away from the center can also be constructed but outer regions of the target appear at a plane other than the exact down range. Consequently utilization of normal representation would suffer from distorted display of targets placed away from the origin.

The maximum representation provides a better display of the results. Since it demonstrates the placement of targets in a more apparent way, this representation will be used in the following sections of the work.

4.2 Rigorous Model

In this part of the work, time domain back projection algorithm is to be applied to data which is obtained directly from the full-wave electromagnetic analysis software. In spite of the fact that both simple and rigorous model utilize same back projection algorithm, the difference occurs in data generation process. For example, antennas are defined pointwise and assumed to be omnidirectional in simple model. In addition, objects are defined as pointwise perfect electrical conductors in simple model. In rigorous model, practical Vivaldi antennas supporting ultra-wide band operation are designed and realized. Furthermore, scatterers are generated as sphere shaped metal objects with 10mm diameter in rigorous model.

After implementing the calibration process, which is explained in Chapter 2, to scattering parameters obtained from CST, back projection algorithm is applied. The resultant image is shown in Figure 4.3(a) where high side lobe levels can be observed. In order to investigate whether the side lobes can be suppressed by using windowing or not, Hamming window ([27]-[28]) is applied to the calibrated data and the results are shown in Figure 4.3(b). It can be seen that Hamming window greatly reduces the side lobe level since average signal level is decreased in non-

target areas. However, signal power corresponding to targets in the corners is also slightly reduced. That is, there exists a tradeoff between image resolution and dynamic range. In spite of this trade-off, the results obtained with Hamming window is preferred and compared with the results obtained with the data generated through simple model in Figure 4.4.

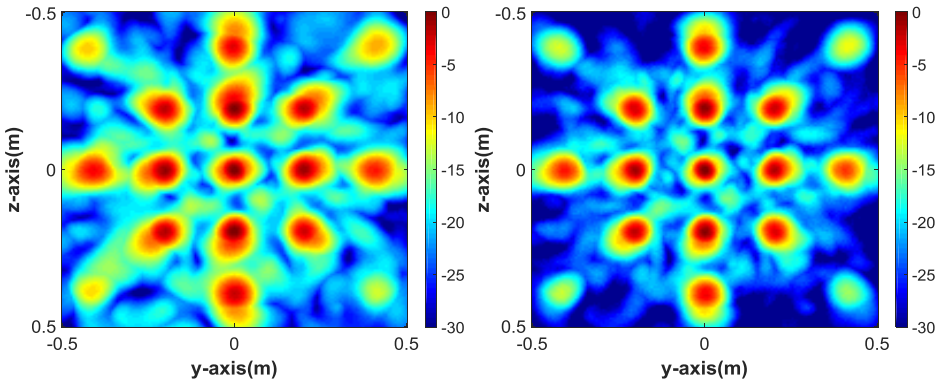

(a) (b)

Figure 4.3 Rigorous model point spread functions obtained by using maximum representation with 17 targets located at x=0.5m (a) without Hamming window (b) with Hamming window

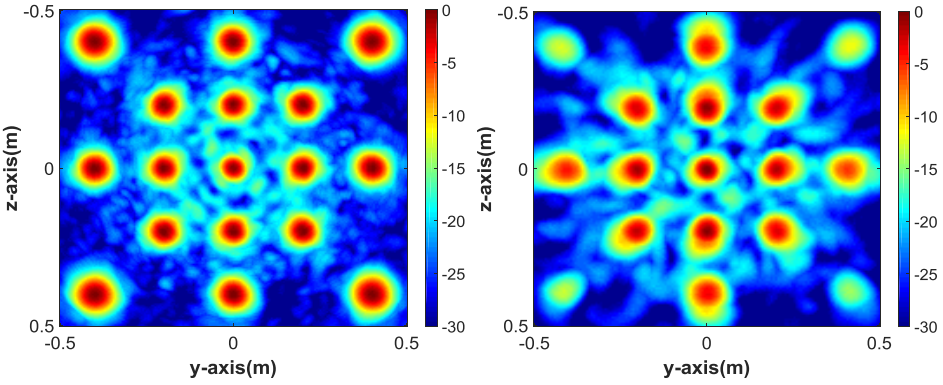

(a) (b)

Figure 4.4 Comparison of images obtained for 17 targets located at x=0.5m (a) simple model (b) rigorous model

The main reasons for the differences between the images obtained with simple model and rigorous model are the MIMO array configuration and the radiation patterns of the antenna elements. When rigorous data is used to back project the middle part of the imaging area, independency of the signals are high enough to obtain fine cross resolution since the region is in the broadside of the aperture. The main advantages of targets placed in the broadside are the lower free space attenuation and higher gain of the antennas in broadside direction. To begin with, travel distances of the electromagnetic waves reflected from targets placed in the broadside of the aperture are lower when compared with reflections from targets in the corners. Hence, attenuation level is lower. In addition to free space attenuation, radiation pattern has a huge impact on the images. Since the power level of the collected waves reflected from the targets on the corners would be decreased due to the fact that they are outside of the broadside of both transmitter and receiver antennas.

In Figure 4.5, two different targets are placed in a single transmitter and receiver antenna system. Target-I is in the broadside direction of the antennas, whereas target-II is out of the major lobes of both antennas. Furthermore, reflected signal from target-I experiences less attenuation due to the shorter path. That is, received power of target-II is decreased by both radiation pattern and attenuation.

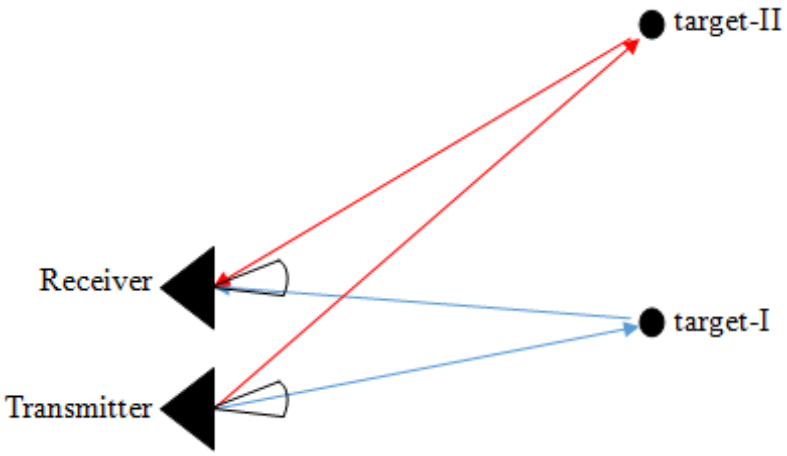

Figure 4.5 Demonstration of different targets affected by radiation pattern

Even though free path attenuation of both cases could be corrected in back projection algorithm which is expressed in equation (2.4), radiation pattern effect cannot be eliminated. In other words, there would always be differences stemming from realization of practical antennas in the environment and taking radiation pattern into consideration between simple and rigorous models. Therefore, addition of radiation pattern into the simple model would provide an improved model which may result in images closer to the ones obtained with rigorous model. If this can be achieved, the performance of a MIMO array configuration can be evaluated efficiently and accurately without needing the use of computationally expensive full-wave analysis.

4.3 Improved Simple Model

As seen from the point spread function results of simple and rigorous models, it is obvious that there exist a lot of differences. From the equations of simple models, only factors which are taken into account are the attenuation due to the spreading loss and phase shift due to the distance that electromagnetic waves travel. Yet, there would be excessive considerations that need to be taken into account in order to obtain the same results with full wave electromagnetic simulations or practical measurements. Since the main purpose of this work is to decrease the complexity and reduce simulation time without conducting a full wave electromagnetic simulation, increasing the variables and making model more complex conflict the idea of the simple model. Thus, only the radiation pattern is utilized as the most dominant practical factor in the development of improved model.

4.3.1 Effect of Radiation Pattern

In order to include the effect of radiation pattern on transmitted and received signals, azimuth and elevation angles between the antenna and the scatterer should

be calculated. In Figure 4.6, antenna and scatterer locations and azimuth and elevation angles are defined.

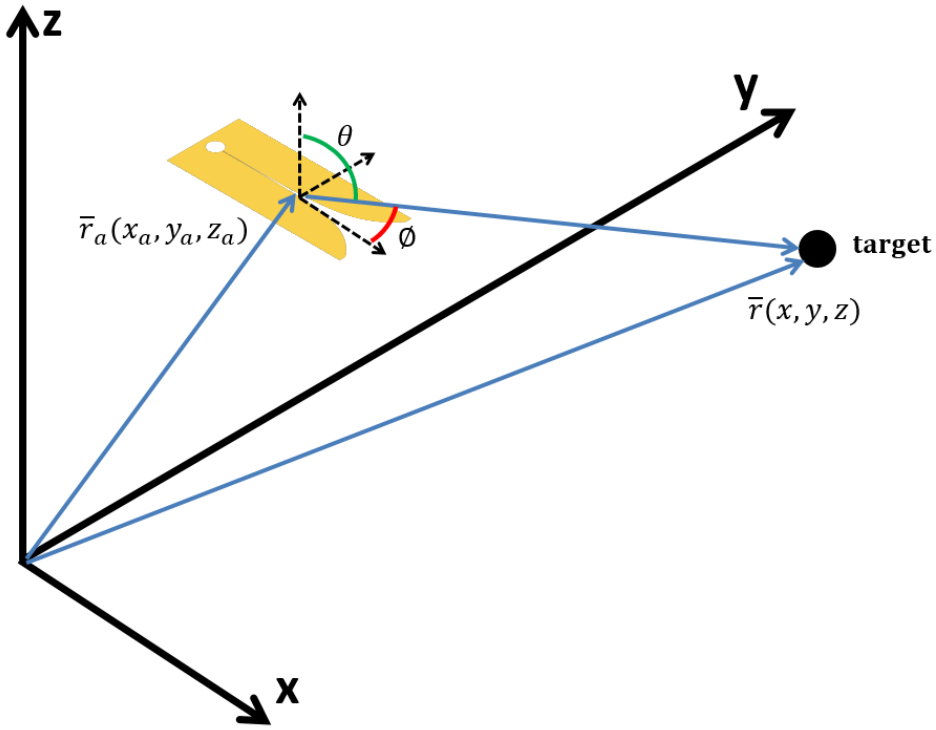

Figure 4.6 Demonstration of antenna and scatterer in cartesian coordinates

Azimuth, ϕ, and elevation, θ, angles could be calculated by using the location of the target, $\bar{r}$ and the location of the antenna, $\bar{r_a}$, as:

$$Azimuth: \emptyset = \tan^{-1}\left(\frac{y - y_a}{x - x_a}\right)$$

$$Elevation: \theta = \sec^{-1}\left(\frac{|\bar{r} - \bar{r_a}|}{z - z_a}\right) \tag{4.1}$$

In Figure 4.7 and Figure 4.8, E- and H- plane radiation patterns of Vivaldi antenna obtained by CST Studio are given, respectively. After calculating the angles, corresponding values of the radiation pattern is used.

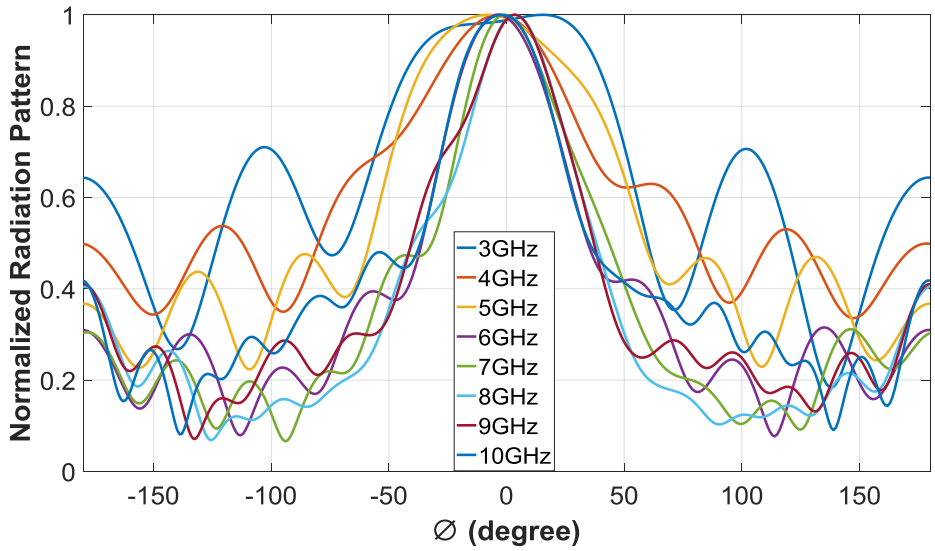

Figure 4.7 Vivaldi antenna E-plane radiation pattern at θ=90°

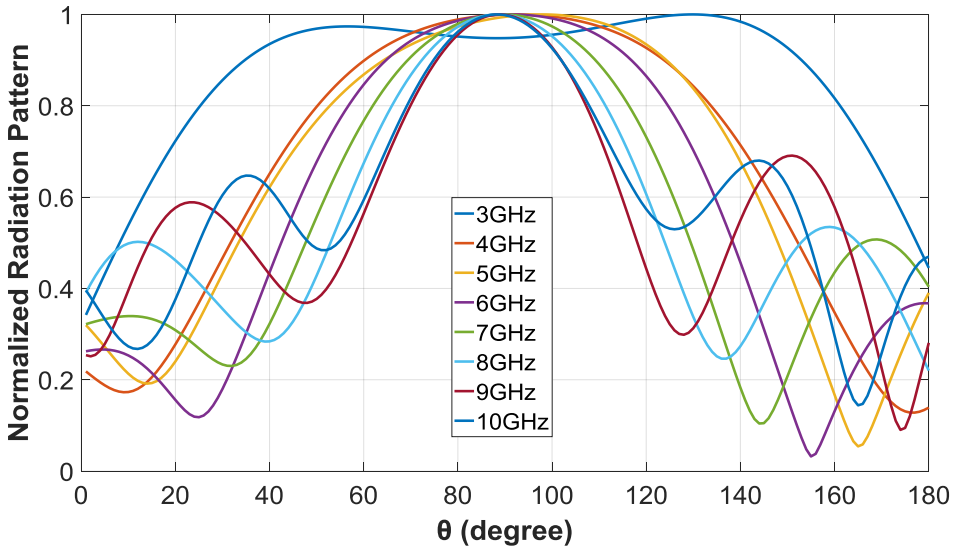

Figure 4.8 Vivaldi antenna H-plane radiation pattern at Ø=0°

As seen from Figure 4.7 and Figure 4.8, radiation pattern data is available only for 8 frequency samples. However the CTS data for which back projection method is applied, comprises 1001 frequency samples. Nearest neighbor interpolation method

is used and as shown in Figure 4.9, for each intermediate frequency sample, the radiation pattern of the closest measured frequency data is used.

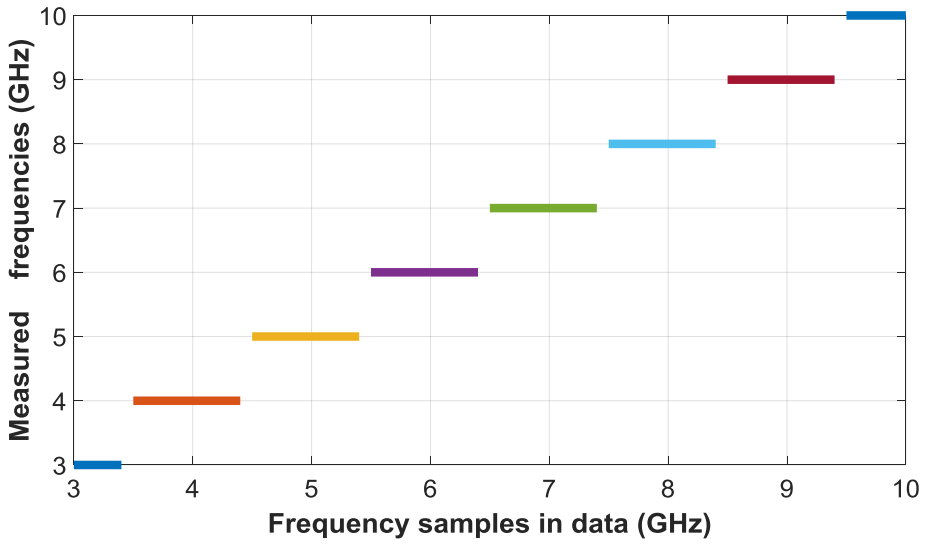

Figure 4.9 Nearest neighbor interpolation for intermediate frequencies

By including the radiation pattern information, improved model is obtained. Thereby, the signal between i^{th} transmitter, j^{th} receiver and l^{th} target at frequency sample f is calculated by:

$$U(t_i, r_J, f, s_l) = \frac{e^{-j\,2\pi\,f\,\tau(t_i,r_j,s_l)}}{d_t(t_i,s_l)\;d_r(r_j,s_l)} F_{t_i,s_l}(\theta_t, \emptyset_t) F_{r_j,s_l}(\theta_r, \emptyset_r) \qquad (4.2)$$

where F_{t_i,s_l} and F_{r_j,s_l} functions represents the radiation patterns for transmitter and receiver antennas at calculated azimuth and elevation angles for the corresponding target.

4.3.2 Results Obtained by Using the Improved Model

The maximum representation of the image obtained for 17 scatterers located at 0.5m from the array aperture by using the data generated by the improved and the simple model are given in Figure 4.10. Even though the images show similarities,

there exists a crucial difference. The targets in the outer parts of the imaging area become less distinct which is a similar phenomenon observed in the rigorous model.

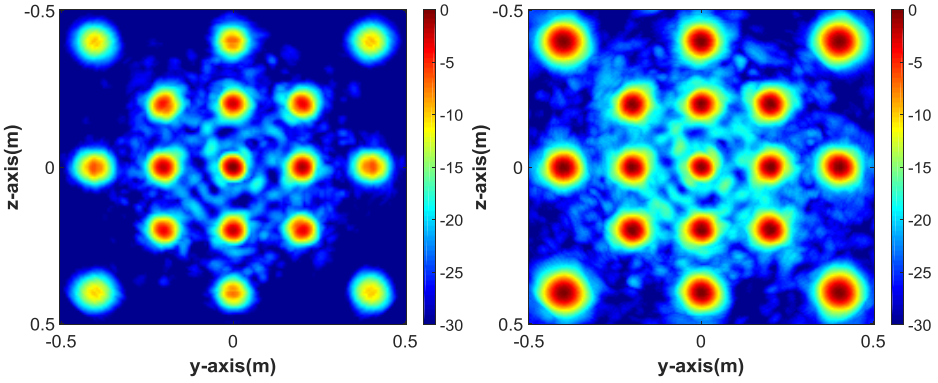

(a) (b)

Figure 4.10 Point spread functions by using maximum representation with 17 targets located at x=0.5m (a) improved model (b) simple model

Received powers corresponding to reflections from targets in the bore sight of the array are not decreased by radiation pattern factor. Therefore, difference between simple and improved model in terms of cross range resolution in bore sight direction is low. On the other hand, outer regions of the imaging plane become distant from the bore sight of the aperture and received powers are significantly reduced due to the radiation pattern. That is, number of effective antennas illuminating and collecting reflected electromagnetic waves from the distant targets is decreased. Since simple model utilizes omnidirectional antennas, number of effective antennas for each target in terms of imaging is same. Thereby, power levels of targets in the point spread functions differ in simple and improved model cases. Even though the overall sidelobe level is decreased unlike rigorous model case, by generating a simple model and developing into improved model considering radiation pattern provide an understanding that such MIMO imaging configuration would suffer from reconstruction of targets outside the bore sight.

4.4 Analysis of Time Domain Signals

Even though point spread functions would give ideas about the system performance, it is crucial to analyze the received data in detail. The reason is that point spread function involves the effect of entire antenna elements. That is, it would be hard to create cause effect relationship between parameters and results. By investigating signals in time domain for transmitter and receiver pairs, how the data is generated is to be observed and importance of ultra wide band usage could be realized.

First, simple and improved simple models are to be analyzed. Since emitted signals are not distorted by practical effects, it is expected that received signals from the targets would correspond to the theoretical calculations. The only difference between simple and improved models is the effect of radiation pattern. Since radiation pattern only affects in terms of magnitude, the time instances of reflections for each model should not change, yet, magnitudes would be different. In order to analyze the time domain signals, a transmitter and receiver pair is chosen. The distance between antenna elements are kept as small as possible so that radiation pattern coefficient could be similar for both antennas. Moreover, an antenna pair close to the origin is chosen for inspection such that reflection from the targets could be analyzed in a more uniform and controlled way. In Figure 4.11, demonstration of chosen transmitter and receiver antenna pair is shown with red and blue colors, respectively.

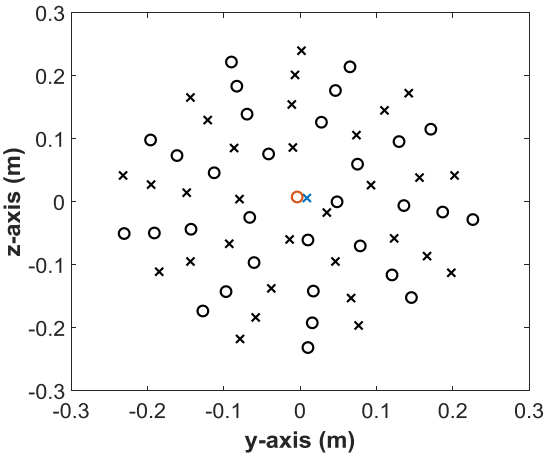

Figure 4.11 Demonstration of active transmitter and receiver pair for time domain signal analyses

4.4.1 Comparison of Simple and Improved Model

According to the travel distances to the chosen antenna pairs, the targets could be categorized into five different groups. Only the first group includes a single target while other groups are comprised of four targets. Each group is expressed with a different color as seen in Figure 4.12.

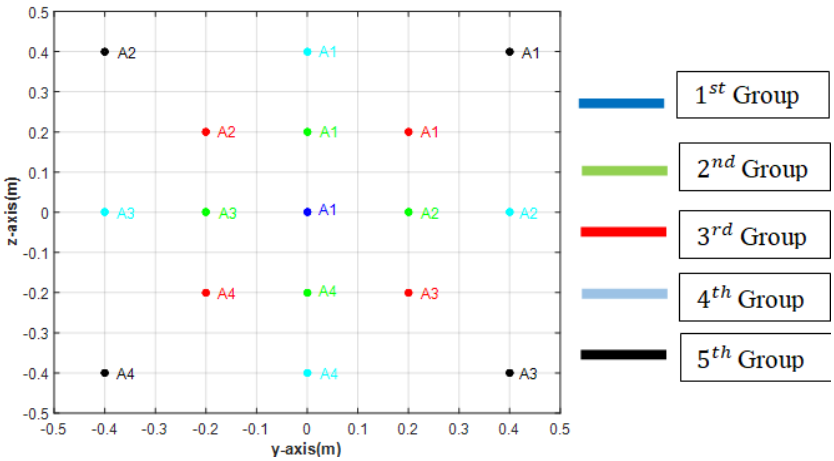

Figure 4.12 Representation of targets belonging to different groups

In order to find the time instances when received signal exhibits a peak, travel durations for each target are calculated. In Table 4.1, expected receive time for each target is listed. Since transmitter and receiver are close to origin, travel duration for the target located at the origin is the shortest. Also, the travel durations for each target in the same group are similar and difference between different groups is apparent.

Table 4.1 Total travel durations from groups

Target Group	**Total Travel Duration (ns)**			
	A1	**A2**	**A3**	**A4**
$\mathbf{1}^{st}$	3.334	-	-	-
$\mathbf{2}^{nd}$	3.574	3.584	3.597	3.608
$\mathbf{3}^{rd}$	3.808	3.820	3.840	3.853
$\mathbf{4}^{th}$	4.240	4.258	4.280	4.299
$\mathbf{5}^{th}$	4.999	5.019	5.049	5.068

In the Figure 4.10, received time domain signals for the chosen antenna pair are given for simple and improved models. The necessity of an ultra-wide band signal in imaging applications is noticed since the signal peaks at certain time locations. Provided that a wider frequency domain signal was used, reflections from each target would be more distinguishable. Since signal with a limited bandwidth spreads in time, different reflections might overlap and seem as a single reflection. For simple and improved models, there exist five different peaks as travel durations are considered.

Due to the free path attenuation, signal level is expected to be reduced for reflections occurred in farther groups. As seen from Figure 4.13, fifth group has the lowest signal level. Yet, the signal level of the first group is lower than second group which contradicts the rule of free path attenuation. The reason why signal level is higher in second division is the accumulation of the reflections from four targets while the first peak is resulted from the single target located at the origin.

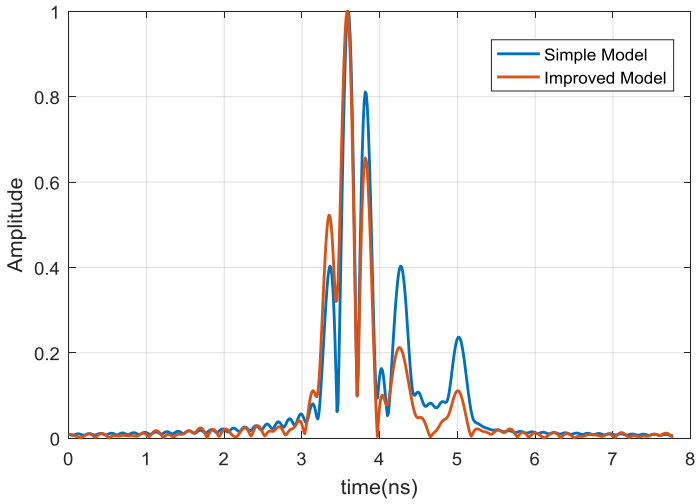

Figure 4.13 Received time domain signal obtained by active antenna pair for simple and improved model

When the result of improved model is observed, it is observed that locations are approximately same with the simple model. Except for the first group, signal levels of the other groups are decreased due to the radiation pattern. The amplitude of the first reflection is not reduced since the target in the origin is located inside the broadside of the antenna where the radiation pattern is maximum. Hence, radiation coefficient corresponding to first reflection is higher than others. Therefore, power level of first reflection is increased in terms of normalized scale.

4.4.2 Analysis of Rigorous Model

As seen from the comparison between simple and improved model in Figure 4.13, addition of radiation pattern does not distort the time domain signal regarding the peak instances. Therefore, one might think that radiation pattern would change the performance of a system in such a predictable way. However, when the images obtained by simple model, improved model and rigorous model are compared as in Figure 4.14, it can be observed that although the targets at the corners became less visible with the improved model similar to the image obtained by rigorous model,

there are still considerable differences with the image obtained by rigorous model. First of all, the sidelobes observed in rigorous model are significantly suppressed in improved model. Secondly, the resolution predicted by the improved model outside the center area is much better than the resolution observed by using the rigorous model. Therefore if the performance of an array configuration is studied by using the improved model and then the array is constructed, the measured performance of the array would be quite disappointing. Therefore, in order to investigate the causes of the differences between the images obtained by the improved and the rigorous models, the time domain signals obtained by both of these models are compared for the same antenna pair and target configuration discussed in the previous section.

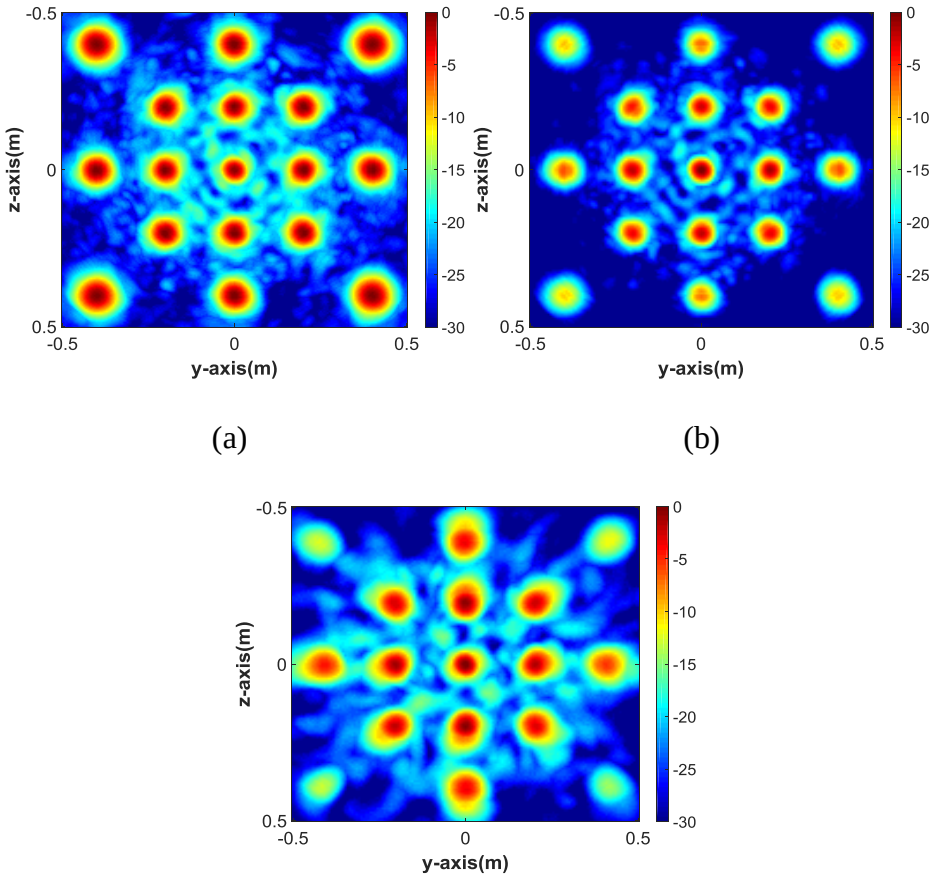

Figure 4.14 Comparison of images obtained for 17 targets located at x=0.5m by three different models (a) simple model (b) improved model (c) rigorous model

Recall that the data obtained from CST needs to be calibrated before feeding into the back projection algorithm. Therefore, first the effects of calibration are demonstrated with the help of the time domain signals. In Figure 4.15, there exists four different time domain data. The “raw data” represents the data obtained from CST. From the simple model, it is expected that first reflected signal from a target would be received after 3ns. However a peak is observed before 1ns. This peak is resulted from direct coupling. In other words, transmitted signal is received before the signal reflected from a target. Since the direct coupled signal dominates the whole signal, the need for calibration is justified. By simply subtracting the measurements obtained from an empty imaging environment, effect of direct coupled signals and reflections from the environment are removed from the data. The result is denoted as “first calibrated data” in Figure 4.15. It can be seen that reflections from 4 groups of targets become more visible after this calibration step. Then this data is calibrated one more time by using the simulation results obtained with a known target (large conducting plate) to remove phase variations in the frequency response of the antenna. This data is labeled as “second calibrated data” in Figure 4.15. After this second calibration, the phase references of the antennas are shifted to the aperture of the array. Due to this phase calibration, time domain data is shifted as can be observed from Figure 4.15. Then, hamming window is applied to second calibrated data. It is seen that sidelobe level of second calibrated data is drastically decreased and peak instances become more apparent.

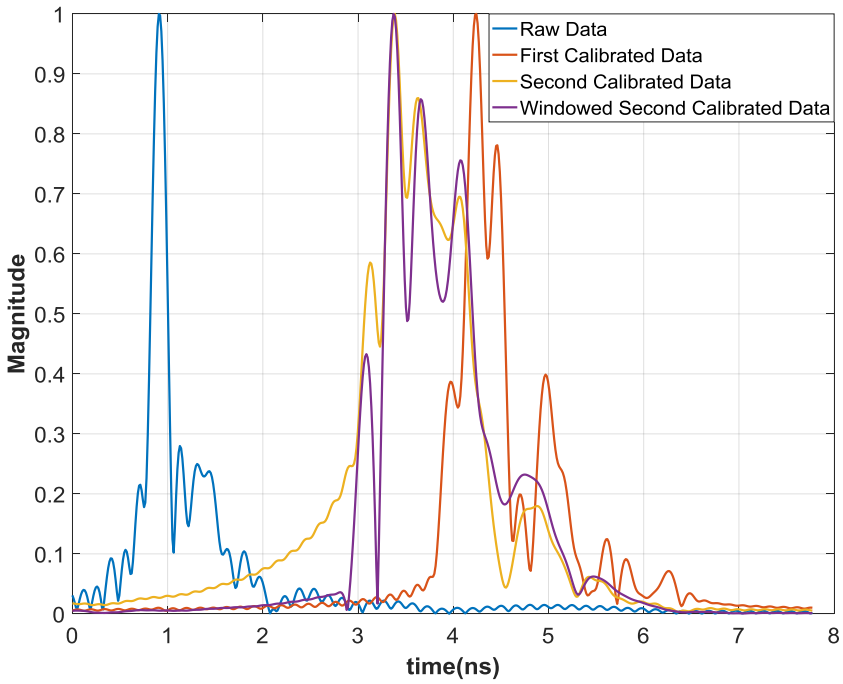

Figure 4.15 Received time domain signals obtained by active antenna pair for rigorous model

4.4.3 Comparison of Improved and Rigorous Models

Time domain signals for improved model and the rigorous model windowed second calibrated data are compared in Figure 4.16.

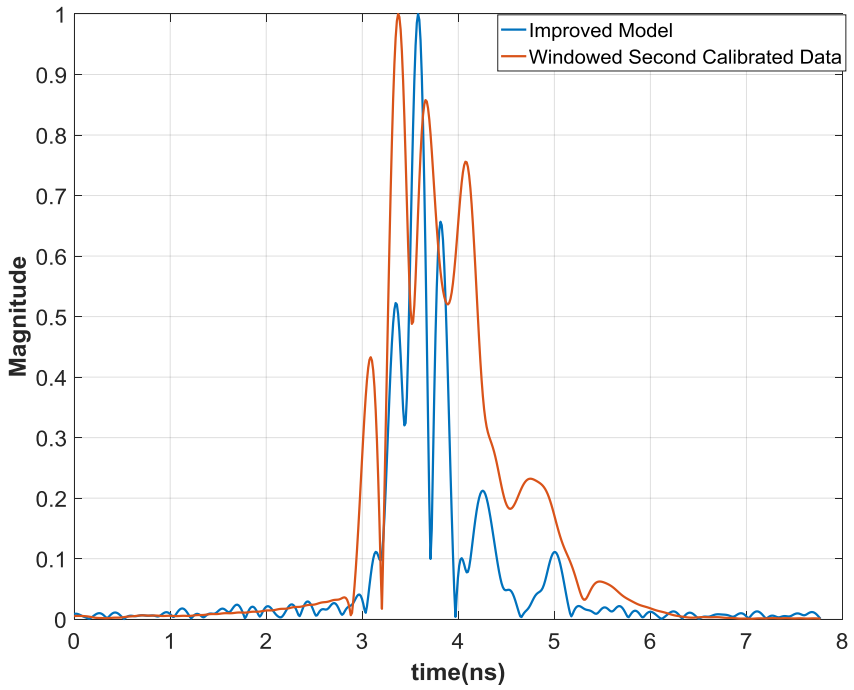

Figure 4.16 Comparison of received time domain signals for improved and rigorous model

In Table 4.2, time instances at which signal peaks are observed are listed for both models. In addition to that, time delays between peaks of improved and rigorous model are given.

Table 4.2 Time instances where received signal peaks for improved and rigorous model

Peak Order	Improved (ns)	Rigorous (ns)	Difference (ns)
1st	3.347	3.088	0.259
2nd	3.581	3.373	0.208
3rd	3.814	3.659	0.155
4th	4.255	4.087	0.168
5th	5.008	4.761	0.247

Even though the first three peaks are similar in terms of shape and power level, rigorous model data differs from improved model data. The most apparent discrepancy is that there exists time difference between received signals. One of the reasons for this difference might be the use of isolated element pattern instead of active element pattern of antennas. Radiation pattern of Vivaldi antennas are simulated in an isolated environment. However, each of the antennas in MIMO configuration performs different radiation characteristics in practice. As a result, improved model in which each antenna possesses identical radiation patterns is not expected to give results same as rigorous model. Another reason is practical modelling of targets. In improved model, targets are point scatterers, on the other hand, they are defined as sphere shaped metals with 10-mm diameter. Thus, total travel distance in rigorous model would be shorter and signals would be received earlier than improved model. Furthermore, there would be multiple reflections between targets or antennas that distort the feature of received signal. By analyzing the time domain received signals, development of improved model with single antenna radiation pattern is not sufficient and additional practical effects should be considered.

CHAPTER 5

MODIFICATIONS ON BACK PROJECTION METHOD BY USING RADIATION PATTERN OF ANTENNAS

In Chapter 4, it is seen that the most effective factor which is ignored in the simple model is the radiation pattern of the antennas. It is confirmed that addition of the radiation pattern to the simple model would make the image result more similar to the images obtained by the rigorous model. In other words, a practical phenomenon is included into the simple model and results became closer to rigorous model promises. Based on this observation it is questioned whether it is possible to make the scatterers at the corners more visible by removing the effects of element radiation pattern in the data obtained by rigorous model during the implementation of back projection algorithm. In other words, knowing that the data obtained by rigorous model is attenuated due to the element pattern, they will be amplified with an amount equal to inverse of the corresponding radiation pattern coefficient. With this modification an improvement in the visibility of the scatterers outside the center region is expected.

In the previous parts, the data generation is conducted in frequency domain since the practical data is obtained in frequency domain. Also, computation cost of generating data in the frequency domain is lower than that of the time domain. Furthermore, the radiation pattern of the Vivaldi antenna is measured in frequency domain. On the other hand, back projection is conducted in time domain due to its computational efficiency. However, the radiation pattern coefficients obtained in frequency domain cannot be applied directly to the time domain data. Therefore, back projection is required to be performed in frequency domain in order to remove the effect of radiation pattern. Therefore frequency domain back propagation algorithm will be introduced in the next section.

5.1 Frequency Domain Back Projection Algorithm

The main difference from time domain back projection is the removal of the inverse Fourier transformation. Since data is already in frequency domain, it is not required to convert the data into time domain. The data between i^{th} transmitter and j^{th} receiver is defined as $\mathrm{U}(\mathrm{t_i}, \mathrm{r_j}, \mathrm{f})$.

Previously introduced imaging environment is repeated in Figure 5.1 for easy reference.

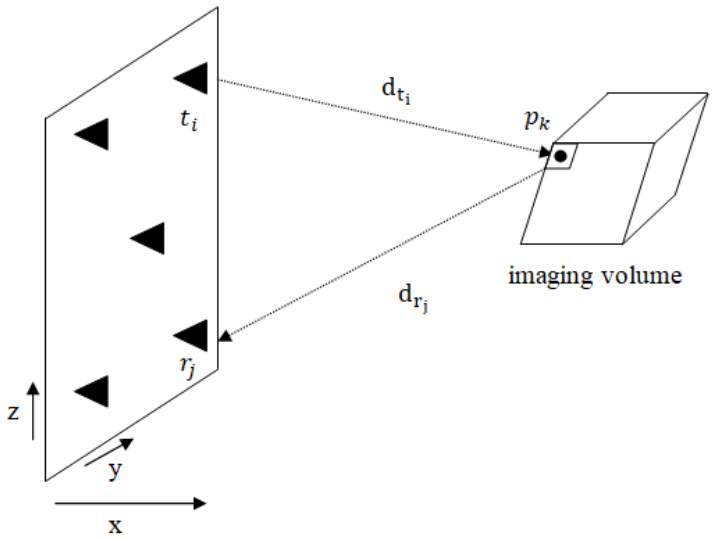

Figure 5.1 Illustration of signal path

Similar to time domain back projection, delay and advance functions are required and calculated by using equation (5.1) and (5.2), respectively.

$$\mathrm{d_t(t_i, p_k)} = \sqrt{\left(\mathrm{x_{p_k}} - \mathrm{x_{t_i}}\right)^2 + \left(\mathrm{y_{p_k}} - \mathrm{y_{t_i}}\right)^2 + \left(\mathrm{z_{p_k}} - \mathrm{z_{t_i}}\right)^2}$$

$$\mathrm{d_r(r_j, p_k)} = \sqrt{\left(\mathrm{x_{p_k}} - \mathrm{x_{r_k}}\right)^2 + \left(\mathrm{y_{p_k}} - \mathrm{y_{r_j}}\right)^2 + \left(\mathrm{z_{p_k}} - \mathrm{z_{r_j}}\right)^2} \quad (5.1)$$

$$\varsigma(\mathrm{t_i}, \mathrm{r_j}, \mathrm{p_k}) = \frac{\mathrm{d_t(t_i, p_k)} + \mathrm{d_r(r_j, p_k)}}{\mathrm{c}} \quad (5.2)$$

During the back projection process in the time domain, each signal is delayed with the corresponding value of the advance function. Hence in the frequency domain, phase shifts corresponding to advance function are removed for each image point by multiplying with $e^{j2\pi f\, \varsigma(t_i, r_j, p_k)}$ term.

$$U_{bp} = e^{j2\pi f\, \varsigma(t_i, r_j, p_k)}\, U(t_i, r_j, f)\, d_t(t_i, p_k)\, d_r(r_j, p_k) \tag{5.3}$$

After finding the back projected signal, the image function corresponding to the k^{th} imaging point is calculated by:

$$m(p_k) = \sum_{t_i} \sum_{r_j} \sum_{f} U_{bp} \tag{5.4}$$

Different from time domain calculation, frequency domain back projection requires additional summation operation on frequency samples.

To eliminate the effects of radiation patterns of transmitter and receiver elements equation (5.3) can be modified as:

$$U_{mbp} = \frac{e^{j2\pi f\, \varsigma(t_i, r_j, p_k)}\, U(t_i, r_j, f)\, d_t(t_i, p_k)\, d_r(r_j, p_k)}{F_{t_i, p_k}(\theta_t, \emptyset_t)\, F_{r_j, p_k}(\theta_r, \emptyset_r)} \tag{5.5}$$

where U_{mbp} represents the modified back projected signal, F_{t_i, p_k} and F_{r_j, p_k} are the corresponding radiation coefficients between i^{th} transmitter, j^{th} receiver and k^{th} image point.

Even though we could compensate the effect of antenna radiation pattern by using equation (5.5), in case that $F(\theta, \emptyset)$ function is close or equal to zero, U_{bmp} would blow up. Hence care must be taken when directly dividing with a function, especially in low signal to nosie ratio (SNR) environments. Since the input data in this scenario is obtained from a simulation software and it is not measured data, the SNR is high and this division does not cause any problem. However it should be noted that a suitable regularization method should be applied [29] in low SNR environments.

5.2 Point Spread Function of Rigorous Model

Before applying the modified back projection algorithm, the results obtained with time domain and frequency domain back projection algorithm are compared to verify the accuracy of the developed code. In Figure 5.2, images obtained by applying back projection in both time and frequency domain to the data generated by rigorous model are presented. As seen from the point spread functions, the results are almost same. Hence, operation of frequency domain back projection is verified.

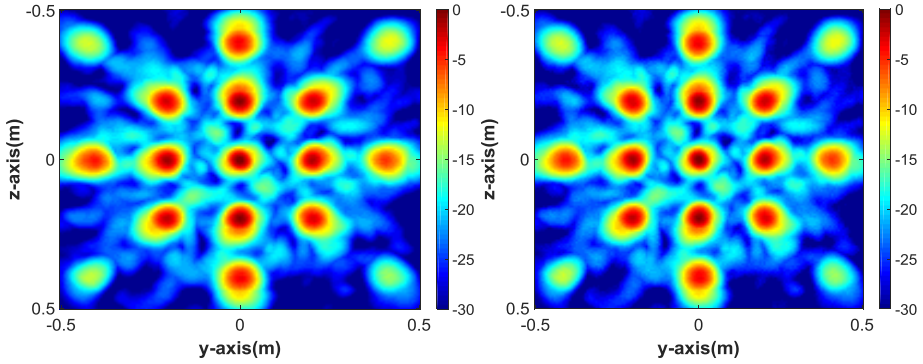

(a) (b)

Figure 5.2 Maximum representation of images obtained by back projection algorithm (a) frequency domain (b) time domain

Then, modified back projection algorithm is applied to the data generated by rigorous model. The obtained image is presented in Figure 5.3 (a), and compared with the traditional back projection result in Figure 5.3 (b).

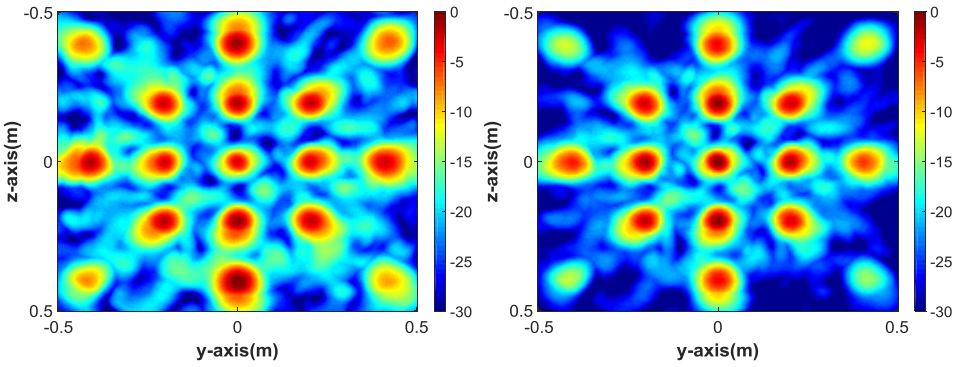

(a) (b)

Figure 5.3 Maximum representation of images obtained by two different frequency domain back projection algorithm (a) modified back projection (b) traditional back projection

As expected, it is seen from Figure 5.3 that targets outside the center region become more visible since effect of radiation pattern is removed. On the other hand, sidelobe level of the image obtained by modified back projection algorithm is higher than the one obtained with traditional algorithm. This may be due to the fact that noise signal is also amplified when the signals are divided with the corresponding radiation coefficients. Therefore, one may conclude that although the scatterers at the corners become more visible with the modified algorithm, it is not preferable due to the increased side lobe levels.

CHAPTER 6

CONCLUSION

As a result of the research in the microwave technology, practical usage of theoretically proven applications are developed. For example, near field imaging systems have been improved in terms of feasibility with the utilization of different techniques such as ultra-wide band signals and MIMO method. However, enhancement of a system in terms of cost and complexity is one of the demands in today' s society. Hence, studies on optimization of such systems should be conducted.

Development of a system could be investigated in three parts which are theoretical calculations regarding the system requirements, utilization of electromagnetic solvers with rigorous models and practical measurements. In case of any undesirable result obtained in practice, one should revise the rigorous model to find the cause of fault. Yet, investigation of errors or development of the system after constructing the system would be time consuming and costly. Hence, priority should be providing the congruity of rigorous models to practical systems. However, taking practical factors into account in the electromagnetic solvers would not benefit as complexity of the system is considered. Therefore, additional analyzes should be performed before generation of rigorous models and effect of the parameters should be observed.

In the initial parts of the work, a simple model of the imaging environment is constructed. With the utilization of back projection method and calculation of point spread function, imaging performance of an ideal system is investigated. The idea is that one should enhance the simple model by taking practical considerations into account and obtain the results of a rigorous model. By adding radiation pattern of antennas into calculations, simple model is revised and improved model is

generated. By comparing point spread functions of improved and rigorous models, it is observed that both model show similarities. For instance, resolution of the targets at the corners severely worsens. The differences between models which are the usage of radiation pattern and effect of calibration in the rigorous model are studied. For example, radiation pattern of a single antenna is used while it is known that element pattern would be different in an array system. Also, radiation pattern at certain frequency samples are used in the generation of improved model. In case one measures radiation pattern of each antenna at every frequency, similarities between improved model and rigorous model would increase. However, such measurements and calculations would not benefit in terms of time and complexity. In other words, one could create a simple model and improve the system with practical factors and realize the possible outcomes that would occur in rigorous model or practice.

In this thesis, a forward model is generated and developed with antenna radiation pattern to analyze the similarities with back projected images of a rigorous model in an ultra-wide band MIMO imaging system. To conclude, a simple forward model generation method is introduced to realize the possible outcomes of a rigorous model.

REFERENCES

[1] B. Steinberg, *Principles of Aperture and Array Systems Design*. New York, USA: Wiley, 1976.

[2] S. Caorsi, A. Lommi, A. Massa and M. Pastorino, "Peak sidelobe level reduction with a hybrid approach based on GAs and difference sets," in *IEEE Transactions on Antennas and Propagation*, vol. 52, no. 4, pp. 1116-1121, April 2004.

[3] V. Murino, A. Trucco and C. S. Regazzoni, "Synthesis of unequally spaced arrays by simulated annealing," in *IEEE Transactions on Signal Processing*, vol. 44, no. 1, pp. 119-122, Jan. 1996.

[4] M. Donelli, A. Martini and A. Massa, "A Hybrid Approach Based on PSO and Hadamard Difference Sets for the Synthesis of Square Thinned Arrays," in *IEEE Transactions on Antennas and Propagation*, vol. 57, no. 8, pp. 2491-2495, Aug. 2009.

[5] D. G. Kurup, M. Himdi and A. Rydberg, "Synthesis of uniform amplitude unequally spaced antenna arrays using the differential evolution algorithm," in *IEEE Transactions on Antennas and Propagation*, vol. 51, no. 9, pp. 2210-2217, Sept. 2003.

[6] C. A. Balanis, Antenna Theory: Analysis and Design, Wiley, 2005.

[7] J. L. Schwartz and B. D. Steinberg, "Ultrasparse, ultrawideband arrays," in *IEEE Transactions on Ultrasonics, Ferroelectrics, and Frequency Control*, vol. 45, no. 2, pp. 376-393, March 1998.

[8] R. J. Fontana, "Recent system applications of short-pulse ultra-wideband (UWB) technology," in *IEEE Transactions on Microwave Theory and Techniques*, vol. 52, no. 9, pp. 2087-2104, Sept. 2004.

[9] L. Jofre *et al*., "UWB Tomographic Radar Imaging of Penetrable and Impenetrable Objects," in *Proceedings of the IEEE*, vol. 97, no. 2, pp. 451-464, Feb. 2009.

[10] A. G. Yarovoy, T. G. Savelyev, P. J. Aubry, P. E. Lys and L. P. Ligthart, "UWB Array-Based Sensor for Near-Field Imaging," in *IEEE Transactions on Microwave Theory and Techniques*, vol. 55, no. 6, pp. 1288-1295, June 2007.

[11] J. D. Taylor, *Ultrawideband radar: applications and design.* Boca Raton, FL:Taylor & Francis, 2012.

[12] X. Zhuge and A. G. Yarovoy, "A Sparse Aperture MIMO-SAR-Based UWB Imaging System for Concealed Weapon Detection," in *IEEE Transactions on Geoscience and Remote Sensing*, vol. 49, no. 1, pp. 509-518, Jan. 2011.

[13] X. Zhuge and A. G. Yarovoy, "Sparse multiple-input multiple-output arrays for high-resolution near-field ultra-wideband imaging," in *IET Microwaves, Antennas & Propagation*, vol. 5, no. 13, pp. 1552-1562, October 2011.

[14] D. Tarchi, F. Oliveri and P. F. Sammartino, "MIMO Radar and Ground-Based SAR Imaging Systems: Equivalent Approaches for Remote Sensing," in *IEEE Transactions on Geoscience and Remote Sensing*, vol. 51, no. 1, pp. 425-435, Jan. 2013.

[15] G. R. Lockwood, Pai-Chi Li, M. O'Donnell and F. S. Foster, "Optimizing the radiation pattern of sparse periodic linear arrays," in *IEEE Transactions on Ultrasonics, Ferroelectrics, and Frequency Control*, vol. 43, no. 1, pp. 7-14, Jan. 1996.

[16] X. Zhuge and A. G. Yarovoy, "Study on Two-Dimensional Sparse MIMO UWB Arrays for High Resolution Near-Field Imaging," in *IEEE Transactions on Antennas and Propagation*, vol. 60, no. 9, pp. 4173-4182, Sept. 2012.

[17] F. Natterer, *The Mathematics of Computerised Tomography*, New York:Wiley, 1986.

[18] X. Zhuge, A. G. Yarovoy, T. Savelyev and L. Ligthart, "Modified Kirchhoff Migration for UWB MIMO Array-Based Radar Imaging," in *IEEE Transactions on Geoscience and Remote Sensing*, vol. 48, no. 6, pp. 2692-2703, June 2010.

[19] J. M. Lopez-Sanchez and J. Fortuny-Guasch, "3-D radar imaging using range migration techniques," in *IEEE Transactions on Antennas and Propagation*, vol. 48, no. 5, pp. 728-737, May 2000.

[20] X. Zhuge and A. G. Yarovoy, "Three-Dimensional Near-Field MIMO Array Imaging Using Range Migration Techniques," in *IEEE Transactions on Image Processing*, vol. 21, no. 6, pp. 3026-3033, June 2012.

[21] V. T. Vu, T. K. Sjogren and M. I. Pettersson, "A Comparison between Fast Factorized Backprojection and Frequency-Domain Algorithms in UWB Lowfrequency SAR," *IGARSS 2008 - 2008 IEEE International Geoscience and Remote Sensing Symposium*, Boston, MA, 2008, pp. IV - 1284-IV - 1287.

[22] A. V. Oppenheim, *Discrete-Time Signal Processing*, Noida, UP, India:Pearson Education India, 1999.

[23] S. Chamaani, M. S. Abrishamian and S. A. Mirtaheri, "Time-Domain Design of UWB Vivaldi Antenna Array Using Multiobjective Particle Swarm Optimization," in *IEEE Antennas and Wireless Propagation Letters*, vol. 9, pp. 666-669, 2010.

[24] W. Wiesbeck, G. Adamiuk and C. Sturm, "Basic Properties and Design Principles of UWB Antennas," in *Proceedings of the IEEE*, vol. 97, no. 2, pp. 372-385, Feb. 2009.

[25] T. Spreng, U. Prechtel, B. Schönlinner, V. Ziegler, A. Meusling and U. Siart, "UWB near-field MIMO radar: Calibration, measurements and image reconstruction," *2013 European Radar Conference*, Nuremberg, 2013, pp. 33-36.

[26] H. Aumann, T. Schmitt and D. Mooradd, "A modification of the two-antenna method to determine the phase center location as well as the gain of a wideband antenna," *2015 IEEE International Symposium on Antennas and Propagation & USNC/URSI National Radio Science Meeting*, Vancouver, BC, 2015, pp. 854-855.

[27] F. J. Harris, "On the use of windows for harmonic analysis with the discrete Fourier transform," in *Proceedings of the IEEE*, vol. 66, no. 1, pp. 51-83, Jan. 1978.

[28] A. Nuttall, "Some windows with very good sidelobe behavior," in *IEEE Transactions on Acoustics, Speech, and Signal Processing*, vol. 29, no. 1, pp. 84-91, February 1981.

[29] H. Engl, M. Hanke and A. Neubauer, Regularization of Inverse Problems, Germany, Dordrecht:Kluwer Academic, 1996.